C. R. Physique 12 (2011) 347–368

Contents lists available at ScienceDirect

Comptes Rendus Physique

www.sciencedirect.com

Quantum Hall effect / Effet Hall quantique

Application of the quantum Hall effect to resistance metrology

Application de l'effet Hall quantique à la métrologie des résistances

Wilfrid Poirier *, Félicien Schopfer, Jérémie Guignard, Olivier Thévenot, Pierre Gournay

Quantum Metrology Group, Laboratoire National de métrologie et d'Essais, 29, avenue Roger-Hennequin, 78197 Trappes, France

ARTICLE INFO

Article history:
Available online 19 May 2011

Keywords:
Fundamental metrology
Electrical metrology
Quantum Hall effect
Semiconductors
Graphene
Fundamental constants of physics

Mots-clés :
Métrologie fondamentale
Métrologie électrique
Effet Hall quantique
Semiconducteurs
Graphène
Constantes fondamentales de la physique

ABSTRACT

The quantum Hall effect (QHE) discovery has revolutionized metrology by providing with a representation of the unit of resistance, R_K, that can be reproduced within a relative uncertainty of one part in 10^9 and is theoretically only linked to Planck's constant h and the electron charge e. This breakthrough also results from the development of resistance comparison bridges using cryogenic current comparator (CCC). The QHE experimental know-how now allows the realization of perfectly quantized Quantum Hall Array Resistance Standards (QHARS) by combining a large number of single Hall bars. In the context of an evolution of the *Système International* (SI) of units by fixing some fundamental constants of physics, the determination of the von Klitzing constant R_K through the use of the so-called Thompson–Lampard calculable capacitor and the realization of refined universality tests of the QHE are of prime importance. Finally, the fascinating graphene material might be a new turning point in resistance metrology.

© 2011 Published by Elsevier Masson SAS on behalf of Académie des sciences.

RÉSUMÉ

La découverte de l'effet Hall quantique (EHQ) a révolutionné la métrologie en fournissant une représentation de l'unité de résistance, R_K, qui peut être reproduite avec une incertitude relative de 10^{-9} et est théoriquement reliée seulement à la constante de Planck h et la charge de l'électron e. Cette révolution s'est également appuyée sur le développement de ponts de comparaison de résistances équipés de comparateurs cryogéniques de courants (CCC). Le savoir-faire expérimental en EHQ permet désormais la réalisation d'étalons de résistance combinant de nombreuses barres de Hall élémentaires en réseaux (QHARS) offrant des valeurs parfaitement quantifiées. Dans le contexte d'une évolution du Système International (SI) d'unités fondée sur la fixation de certaines constantes de la physique, la détermination de la constante de von Klitzing R_K, qui utilise l'étalon calculable de capacité de Thompson–Lampard, et la réalisation de tests d'universalité de l'EHQ plus précis sont essentiels. Enfin, le graphène, nouveau matériau fascinant, pourrait marquer un nouveau tournant de la métrologie des résistances.

© 2011 Published by Elsevier Masson SAS on behalf of Académie des sciences.

* Corresponding author.
E-mail address: wilfrid.poirier@lne.fr (W. Poirier).

1631-0705/$ – see front matter © 2011 Published by Elsevier Masson SAS on behalf of Académie des sciences.
doi:10.1016/j.crhy.2011.04.008

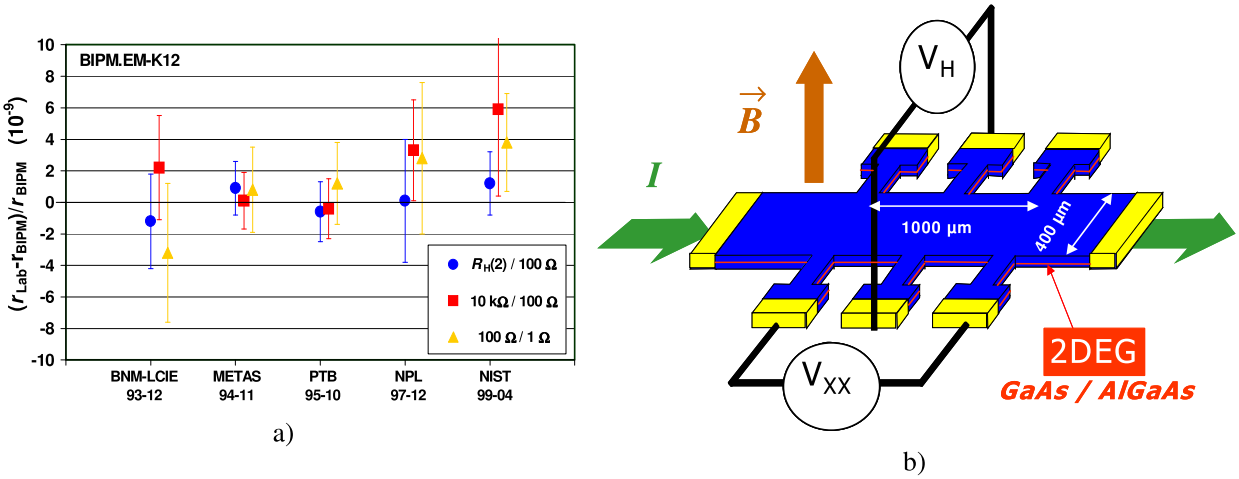

Fig. 1. a) Bilateral comparisons of resistance between several NMIs and BIPM from Ref. [3]. b) Drawing of a Hall bar sample based on a GaAs/AlGaAs heterostructure.

1. Impact of the QHE on the SI units

1.1. The QHE as a representation of the ohm

Before 1990, the ohm was maintained in each country by a set of wire resistors the resistance of which was deduced from the henry or the farad by use of a quadrature bridge. The relative dispersal of the ohm representations was amounting to about one part in 10^6. Only ten years after the discovery of the quantum Hall effect (QHE) by K. von Klitzing in 1980 [1], the *Comité international des poids et mesures* (CIPM) recommended the maintaining of the unit of resistance by use of the QHE [2]. Fig. 1a gathers the results of bilateral comparisons [3] of resistance realized between BIPM and several National Metrology Institutes (NMIs) equipped with QHE setups and cryogenic current comparators (CCC). These data reveal a degree of equivalence of NMIs as low as some parts in 10^9, i.e. three orders of magnitude better than previously. This is a direct consequence of the universality property of the QHE.

This quantum phenomenon appears in a two-dimensional electron gas (2DEG) placed in a perpendicular magnetic field. Let us consider a sample of the typical shape which is a bar with lateral contacts, as shown in Fig. 1b. One can define the so-called Hall resistance R_H and the longitudinal resistance R_{xx} by:

$$R_H = V_H/I \quad \text{and} \quad R_{xx} = V_{xx}/I \tag{1}$$

The QHE gives rise respectively to plateaus for the Hall resistance and to oscillations of the longitudinal resistance (the Shubnikov–de Haas oscillations) when varying the magnetic induction, as shown in Fig. 2a. The quantized values of R_H on the plateaus are given by:

$$R_H = R_K/i \tag{2}$$

i is the plateau index, it is an integer, R_K is the von Klitzing constant, theoretically equal to h/e^2 where h and e are the Planck's constant and the electron charge respectively. Whereas R_H is quantized on a plateau R_{xx} simultaneously drops to zero. This latter feature reveals a dissipation-less state of the 2DEG without any backscattering. These quantum properties can be observed in a sample based on a 2DEG fabricated from a GaAs/AlGaAs semiconductor heterostructure for instance, pierced by a strong magnetic flux density ($\approx$ 10 T) and cooled down to low temperature (1.5 K). Although the reproducibility of R_K was checked within some parts in 10^{10}, its determination in the *Système International* (SI) of units has an uncertainty of one part in 10^7. It is the value of the Hall resistance quantized on the plateau which is used as a reference to calibrate resistances. The calibration of a resistor consists in comparing the Hall resistance R_K/i (the $i = 2$ plateau is usually used) with that of the resistor by using a resistance comparison bridge. The resistance is thus determined in terms of R_K. However, because of the universal property of the QHE and for practical reasons, the R_K uncertainty (10^{-7}) is conventionally dropped out in calibration certificates. Thus, resistors are calibrated in terms of an officially agreed exact value of R_K, presently named $R_{K\text{-}90}$, which was set taking into account experimental determinations of R_K and of the h/e^2 ratio. Fig. 2b shows the tracking of a 100 Ω wire resistance standard realized by QHE: around a linear drift the standard resistance can be stable within some parts in 10^9.

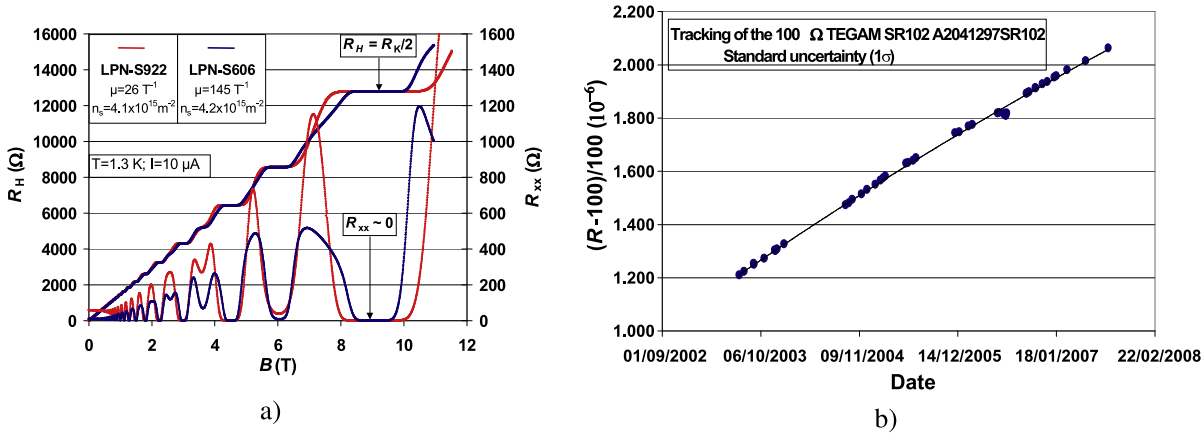

Fig. 2. a) Magneto-resistance curves of GaAs/AlGaAs Hall bar samples. b) Tracking of a 100 Ω wire resistor in terms of R_{K-90}.

1.2. The QHE as a corner stone of the new SI

The QHE, as well as the Josephson effect [4–6] which provides a quantum representation of the volt based on the phenomenological constant K_J, the Josephson constant theoretically equal to $2e/h$, have revolutionized the representation of electrical units. The possibility to directly link the ampere to the electron charge e by means of electron pumps, based on the Coulomb blockade [7,8], another major quantum effect in condensed matter, is even extensively investigated. These electron pumps deliver a quantized current equal to Q_X (the tunneling charge, theoretically equal to e or $2e$) times a pumping frequency f. The breakthrough lies on the universality and high reproducibility of these quantum effects, intrinsically related to h and e constants. Moreover, they have inspired metrologists thinking about the evolution of the SI towards a "natural" system in which, more precisely, all base units should be defined by fixing some constants of physics $(h, e, c, k_B, \ldots)$ [9]. One unit particularly draws the attention of metrologists and is a great stake: the kilogram. Actually, in the present SI, it is the unique unit still defined using a material artefact: the international prototype of the kilogram. From comparisons with mass of copies fabricated also in 1875, it is believed that the kilogram could drift in an ineluctable way (about 5 parts in 10^{10} per year). One of the proposed routes to redefine the kilogram is to link it to the electrical units by means of the watt balance which consists in comparing an electrical power to the mechanical power of a moving mass in a gravity field (Fig. 3a) [10–12]. This route has the big advantage of benefiting from the high-quality quantum representations of the electrical units. If the relationships for the von Klitzing constant $R_K = h/e^2$ and for the Josephson constant $K_J = 2e/h$ are validated, this experiment would lead to the redefinition of the kilogram in terms of the Planck's constant h. This "electrical" kilogram would symbolize a crowning achievement for the quantum electrical metrology and particularly for the metrological application of the QHE. Before establishing such a new SI, several challenging objectives have to be reached. One of the major issue is the validation of the relation $R_K = h/e^2$. This implies the independent SI determinations of h/e^2, which are nothing else but determinations of the fine structure constant α, and of the von Klitzing constant R_K. The latter is based on the use of the Thompson–Lampard capacitor [13]. The determination of some fundamental constants of physics is also an issue before fixing them. The QHE will contribute to the determination of the Planck's constant h through the watt balance experiment, and also to the determination of the electron charge e in closing the metrological triangle. This experiment (Fig. 3b) can be reduced to the implementation of Ohm's law where the voltage is derived from the Josephson effect, the resistance is measured in the QHE regime and the current is delivered by electron pumps. Considering the crucial role that QHE is expected to play in all these projects, it is of prime importance to improve its experimental mastery, to deepen its understanding, and in other words to reinforce the confidence in it. For that purpose, quantization tests of the QHE in peculiar materials like graphene, and/or with an accuracy never reached so far (a few part in 10^{12}) are very interesting and fruitful [14]. Such tests are also nothing else but tests of the fundamental aspects of the QHE theory. The above described experiments are the new challenges that QHE metrology and, more generally, quantum electrical metrology has to take up.

2. The QHE: from the theory to the practical metrological implementation

2.1. Theoretical basis of the QHE

The quantization of the Hall resistance of a two-dimensional electron gas is related to the quantization of the density of states in Landau levels in presence of a magnetic field. The Landau levels occur at energies which are the eigenvalues of the Hamiltonian of an electron including a potential vector:

$$H = \frac{1}{2m^*}(p + eA)^2 \tag{3}$$

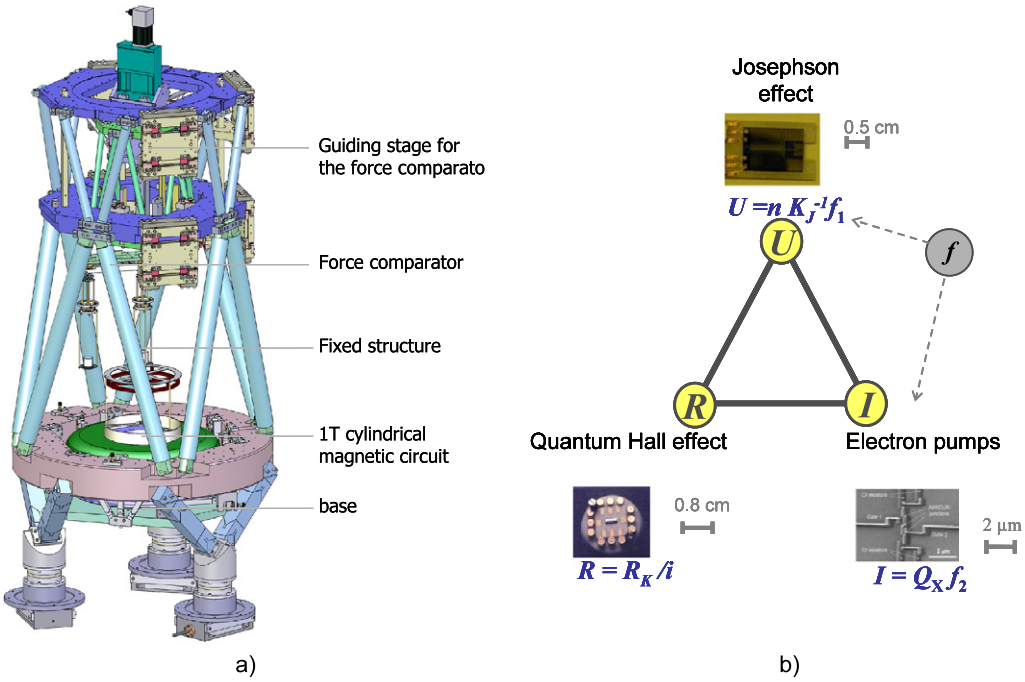

Fig. 3. a) Drawing of the LNE watt balance (under construction) by courtesy of F. Bielsa (e-mass project meeting at PTB). b) Sketch of the principle of the quantum metrological triangle experiment.

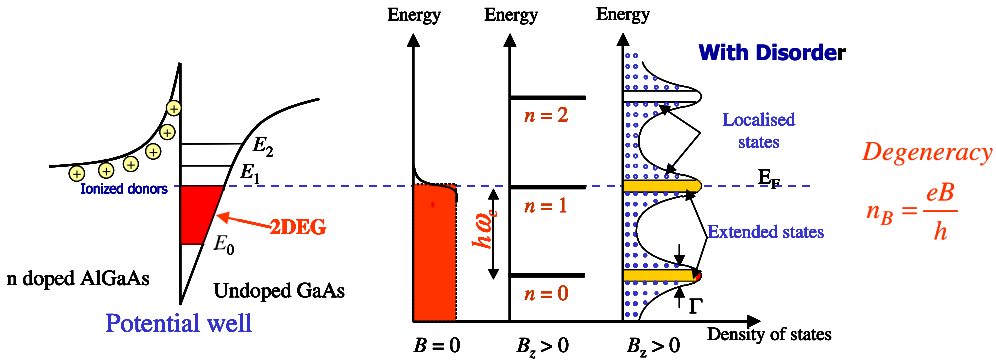

Fig. 4. Landau levels and density of states for one spin value in absence and presence of disorder in GaAs.

A is the potential vector associated to the magnetic field, p is the momentum operator, m^* the effective mass of the electron. To simplify this introduction to QHE, the Zeeman effect, which lifts the degeneracy of Landau levels, is not considered. This Hamiltonian can be reduced to that of a harmonic oscillator. The energy of the nth Landau level is:

$$\varepsilon_n = \hbar\omega_C(n + 1/2) \tag{4}$$

with $\omega_C = eB/m$ the pulsation of the cyclotron motion of the electron.

The density of states (Fig. 4) is a semi-infinite Dirac comb with positive energies and an energy step $\hbar\omega_C$ (the cyclotron energy). Landau levels are highly degenerated with respect to the center of guidance of the cyclotron orbit. In fact, the area occupied by a state (electron) in each Landau level is $2\pi l_B^2$ where $l_B = \sqrt{\hbar/(eB)}$ is the magnetic length. This area corresponds to the area threaded by one magnetic flux quantum:

$$2\pi l_B^2 = \frac{h}{eB} = \frac{\phi_0}{B} \tag{5}$$

This emphasizes the fact that the phase space corresponds to the physical plane in the QHE regime. From the area of an electron state in a Landau level, it is straightforwardly deduced that the density of states per surface unit of one Landau level for one spin value is the density of flux quanta n_B:

Table 1
Numerical values of QHE-relevant quantities in GaAs at $B = 10$ T.

ω_C	$\hbar\omega_C$	l_B	n_B
2.65×10^{13} rad s^{-1}	17.5 meV	8.1 nm	2.42×10^{15} m^{-2}

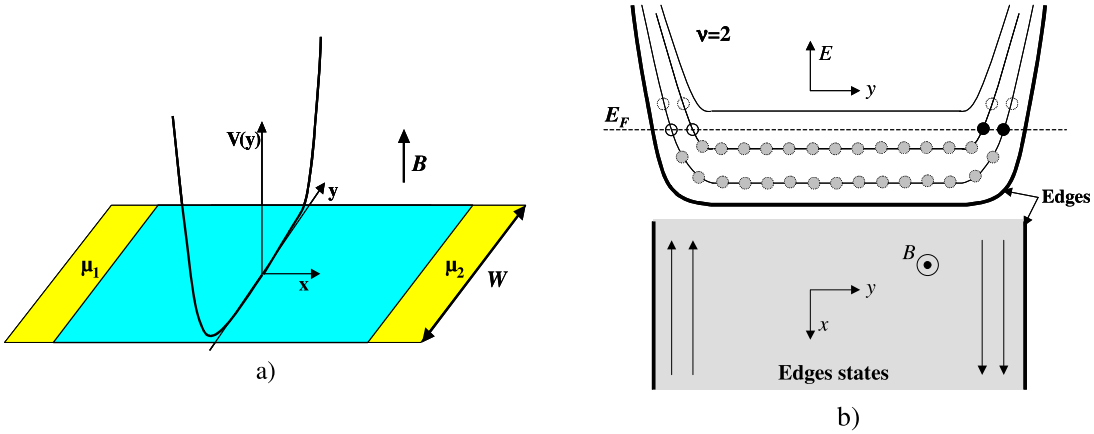

Fig. 5. a) Hall bar sample with two current contacts behaving as electrons reservoirs at chemical potential μ_i. Representation of the confining potential. b) Bending of Landau levels and chiral edges states for $\nu = 2$.

$$\frac{1}{2\pi l_B^2} = \frac{eB}{h} \tag{6}$$

This is nothing else but the degeneracy of the Landau level. A finite energy $\hbar\omega_C$ is necessary to add one additional electron in a higher Landau level: this makes the electronic fluid incompressible. It is useful to introduce the filling factor ν defined by the ratio $\nu = n_S/n_B$, with n_S the density of electrons. For $\nu = 1$, all states of the first Landau level ($n = 0$) at energy $\hbar\omega_C/2$ are occupied, there is one flux quantum per electron. For $\nu = 2$, states of both the two first Landau levels ($n = 0$ and $n = 1$) are filled, there are two electrons per flux quantum. In order to vary the filling of Landau levels it is possible to tune either the magnetic field or the carrier density.

Table 1 gives numerical values considering $B = 10$ T and $m^* = 0.067m_e$ (GaAs). The magnetic length is therefore the smallest characteristic length of the problem. At 1.5 K, the cyclotron energy is two orders of magnitude larger than the thermal energy.

The formation of Landau levels being established, a finite quantity of disorder has to be introduced to explain the existence of quantized Hall plateaus and simultaneous drop to zero of the longitudinal resistance with a finite width when varying the filling factor. In presence of a magnetic field, the disorder which breaks the translation invariance symmetry lifts the degeneracy of the Landau levels, the value of which was previously calculated to be eB/h. Landau levels are broadened and localized states appear in between them. Fig. 4 shows the energy spectrum consisting of localized states between Landau levels and delocalized (or extended) states at the center of the Landau peaks. Both kinds of states play a crucial role in QHE. Delocalized states carry the current and localized states ensure the existence of a gap of mobility. It results that the Fermi level can vary continuously between two Landau energy levels without any change of the Hall resistance. When considering finite size systems with realistic boundaries, extended states appear close to the edges of the device. They are located in the region where the Landau levels bent by the confining potential (Fig. 5a) at the edges intercept the Fermi energy. They are the so-called edge states (Fig. 5b). On each edge of the sample, their number corresponds to the number of filled Landau levels. These one-dimensional states carry electrons in only one direction which depends on the direction of the magnetic field (edge states are chiral). Moreover, the group velocities of states of opposite edges have opposite signs. Consequently, edge states with opposite momentum are spatially separated. The backscattering of electrons filling the edge states is therefore canceled since the probability that an electron crosses the sample by tunneling effect is negligible. It should be mentioned that not only "edges states" but also "bulk states" at energy close to the center of Landau levels are important in quantum Hall systems. Both types of extended states have to be considered to determine the local density of current in the sample. However, referring to the Einstein's relationship, the conductance in the QHE regime can be deduced from the diffusion currents which are carried by electrons in edges states only. The net Hall current in response to the Hall voltage drop thus results from the non-equilibrium occupancy of edge states. The transport in the QHE regime can be described using the edge state picture by means of the Landauer–Büttiker formalism [15]. In such a picture, each edge state is thus a perfect ballistic one-dimensional conduction channel with a transmission probability equal to unity because of the absence of backscattering. Although the disorder can mix edge states of the same edge, scattering backwards is forbidden beyond distances large compared to l_B. The conductance of each one is e^2/h (one spin direction). From this description, one deduces again that R_K, the quantized value of R_H on the first plateau, is h/e^2. The quantization

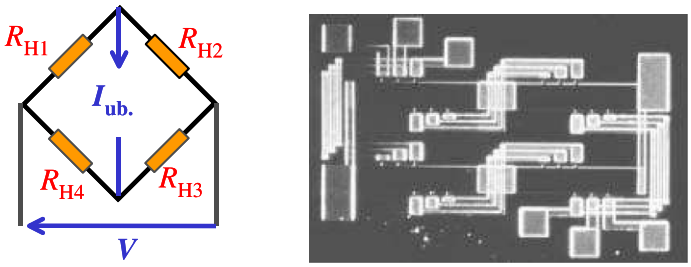

a) b)

Fig. 6. a) Drawing of a Wheatstone bridge. b) Picture of an integrated on-chip Wheatstone bridge defined by lithography in GaAs/AlGaAs 2DEG.

of R_H therefore appears as a direct consequence of the absence of backscattering, or in other words of dissipation in the conductor. This explains the simultaneous drop to zero of the four-terminal longitudinal resistance R_{xx}. Reversely, a finite R_{xx} value is related to the existence of backscattering between the opposite edge states *via*, for instance, tunneling processes and leads to a deviation of R_H from the quantized value. This absence of backscattering conjugated with the scale invariance property of the resistance in 2D makes the Hall resistance independent of the particular shape of the sample in the QHE regime. This is an essential character of the universality of the quantum Hall resistance standard.

Beyond, the fundamental universality property of the QHE, which emerges also in the fact that R_K only depends on e and h, is supported by very strong theoretical arguments [16]. Laughlin [17] first demonstrated that it was a direct consequence of the Hamiltonian gauge invariance property. The robustness of the equality $R_K = h/e^2$ was then generalized by showing that the Hall conductance is a topological invariant [18] and is not sensitive to any gravitational field [19]. As previously pointed out, edge states theory of Büttiker emphasizes that quantization accuracy is a direct consequence of absence of backscattering. More generally, QHE relies on Pauli and Heisenberg principles, combined with the chirality property due to magnetic field. The edge states theory also shows that QHE is a macroscopic quantum effect since phase coherency is required only over the magnetic length scale: inelastic scattering reinforces the quantization by equilibrating the chemical potentials of edge states. Nevertheless, very recently, theoretical quantum electrodynamics (QED) calculations have predicted a deviation of R_K to the ratio h/e^2 related to the screening of the electron charge under high magnetic field [20]:

$$R_K^{-1} = \frac{e^2}{2\pi\hbar}\left[1 + \frac{2\alpha}{45\pi}\left(\frac{\hbar e B}{c^2 m^2}\right)^2\right] \tag{7}$$

Even if the deviation is very tiny, amounting to one part in 10^{20} under magnetic inductions as high as 40 T, this work demonstrates that non-universal correction may exist. It confirms the interest for performing QHE universality tests. It also worth noting that a similar correction has been predicted for the Josephson effect [21].

2.2. The QHE quantization tests

Before recommending the QHE to maintain the ohm unit, testing its universality property was an inescapable prerequisite. To test this universality property, metrologists carried out many comparisons of the Hall resistance obtained with different semiconductor samples. One of the most relevant universality tests consisted in measuring the ratio of the Hall resistances on the $\nu = 2$ plateau in GaAs/AlGaAs sample and on the $\nu = 4$ plateau in Si-Mosfet samples [22]: $R_H(\nu = 2, \text{GaAs})/R_H(\nu = 4, \text{Si-Mosfet}) = 2[1 - 0.22(3.5) \times 10^{-10}]$. A similar degree of agreement was obtained for the Hall resistances of GaAs and Si-Mosfet samples both measured on the $\nu = 4$ plateau [23]. No significant deviation was observed as well between standards based on GaAs/AlGaAs and InGaAs/InP heterostructures [24] within a relative uncertainty of 2.4 parts in 10^8. The robustness of the universality property was also tested in GaAs/AlGaAs 2DEG by varying several parameters: channel size of the Hall bar, electronic mobility of the 2DEG or index plateau number [25]. The conclusion of all these works is that there is no lack of universality of the QHE realized in semiconductor 2DEG within some parts in 10^{10}. More recently, a new technique has been developed which enable very accurate comparisons of quantized Hall resistances having close values: the quantum Wheatstone bridge (Fig. 6a). The idea is quite obvious: by connecting four multiterminal Hall bars in a Wheatstone bridge structure and measuring the unbalance current (voltage) I_{ub} (V_{ub}) of the bridge it is possible to compare the four Hall resistances since:

$$I_{ub}/I = V_{ub}/V \approx \frac{1}{4}\left[(\alpha_1 + \alpha_3) - (\alpha_2 + \alpha_4)\right] \tag{8}$$

where α_j $(j = 1, \ldots, 4)$ is the relative deviation of the jth Hall resistance to its nominal value.

Any discrepancy can be described, with a simple model, by the relative resistance deviation of one resistor among the others:

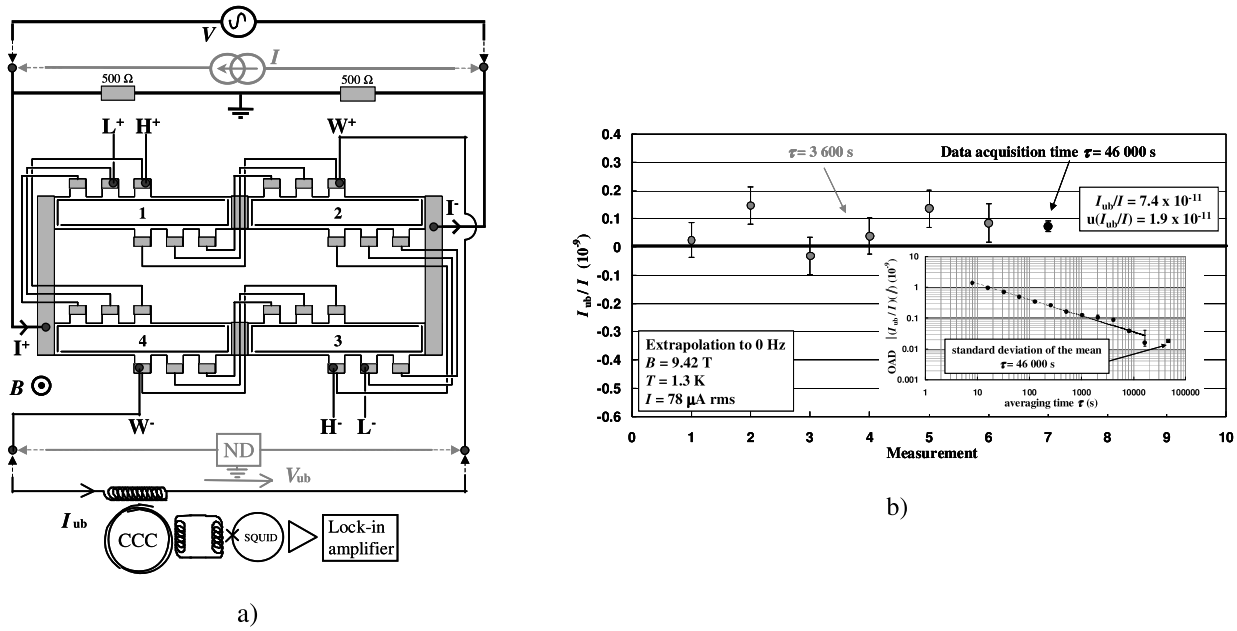

Fig. 7. a) Connection scheme and measurement set-up of a quantum Wheatstone bridge. b) Measurements of the relative unbalance current I_{ub}/I when the device works on the $\nu = 2$ Hall plateau with $I = 78$ µA rms.

$$\Delta R/R = 4 \times (I_{ub}/I) = 4 \times (V_{ub}/V) \tag{9}$$

The accuracy of the technique is based on the multiple connection technique [26]. This technique is described in more details in Section 3.3. Based on fundamental properties of the QHE (drop to zero of the longitudinal resistance on the Hall plateaus, 2-terminals resistance of any system in the QHE regime equal to R_H, chirality of the edges states, etc.), it consists in connecting multiterminal QHE devices with redundant links. It allows the interconnection resistance effect to be canceled: the higher the number of redundant connections, the lower the resistance effect of links. Consequently, this technique allows the combination of several Hall bars in arrays, the resistance of which is quantized with a very high accuracy (some parts in 10^9 or better). The quantum Wheatstone bridge technique has several advantages. Firstly, the comparison takes place *in situ* in a single cryostat, thus avoiding noisy lengths of cables. Secondly, it reduces the resistance comparison to the measurement of an electrical current which can be performed favorably by using a cryogenic current comparator (CCC, see Section 4 for description) equipped with a SQUID. As a proof of this concept of measurement, the technique was firstly implemented in a fully integrated device fabricated in a GaAs/AlGaAs 2DEG.

Fig. 6b shows a picture of this on-chip Wheatstone bridge [27]. The device, a two series array of two Hall bars set parallel to each other, consists of four 400 µm wide connected using the quadruple connection technique. Fig. 7a shows a drawing of the whole measurement set-up. By biasing the bridge with a low frequency (0.5 Hz) voltage and using lock-in techniques, the unbalance current is detected at the terminal-pair (W^+, W^-) with a CCC used as a current amplifier. With a CCC having a sensitivity of 13.6 µA turns/ϕ_0 fitted with an RF SQUID (white noise amounts to $10^{-4}\phi_0/\mathrm{Hz}^{1/2}$) and a 3436 turns detecting winding, the current resolution is 400 fA/Hz$^{1/2}$.

Quadratic frequency corrections are applied to extrapolate measurements to DC regime. Fig. 7b shows several measurements of I_{ub}/I carried out with a supplying current of 78 µA rms. Allan variance analysis proves that the experimental noise is dominated by the white noise throughout the experiment time (insert Fig. 7b). So, the following resistance deviation was deduced: $\Delta R/R(I = 78\ \mu\mathrm{A}) = (29.6 \pm 7.6) \times 10^{-11}$. None of the four quantum resistances departs from the others by more than 30×10^{-11} with a standard uncertainty, never achieved so far, of 7.6×10^{-11}. Complementary work showed that the significant discrepancy observed was probably due to an underestimated correction linear in frequency. This work validated the multiple connection technique and beyond demonstrated the ability of the quantum Wheatstone bridge technique to implement accurate Hall resistance comparisons. In a more recent experiment [28], this technique was successfully used to check the reproducibility of the QHE in GaAs/AlGaAs 2DEG with the record standard uncertainty of 4 parts in 10^{11} [article in preparation]. These works demonstrate that a QHE Wheatstone bridge made of three identical Hall bars and a fourth one of different nature should allow the realization of universality tests of the QHE with uncertainties down to some parts in 10^{12} using a less noisy CCC. Such experiments are very interesting in the context of the SI redefinition.

2.3. Experimental conditions for the metrological implementation of the QHE

Because experimental conditions of the QHE operation discard from theory, the reproduction of R_K with a relative uncertainty less than 10^{-9} is obtained only if specific criteria of quantization are fulfilled. These criteria are defined in technical

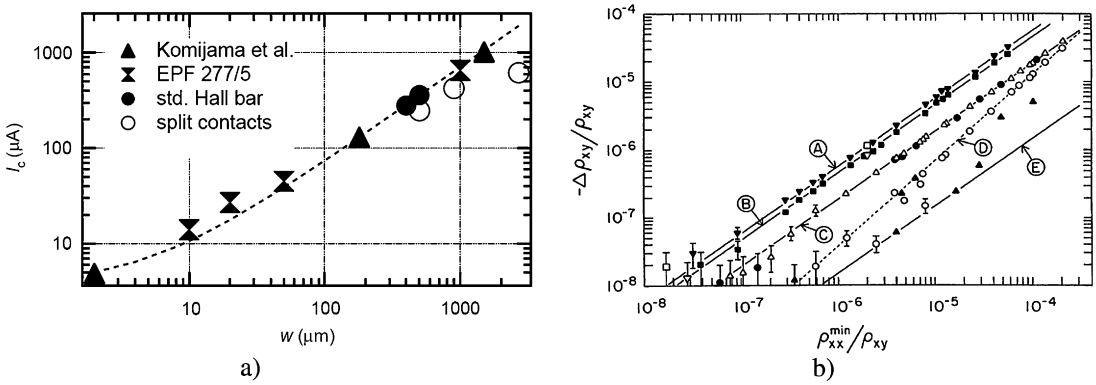

Fig. 8. a) QHE breakdown current measured as a function of the width of the conduction channel in GaAs samples from Ref. [30]: the breakdown current increases with the width of the channel. b) Relative deviation $\Delta\rho_{xy}/\rho_{xy}$ versus $\rho_{xy}^{\min}/\rho_{xy}$ from Ref. [31].

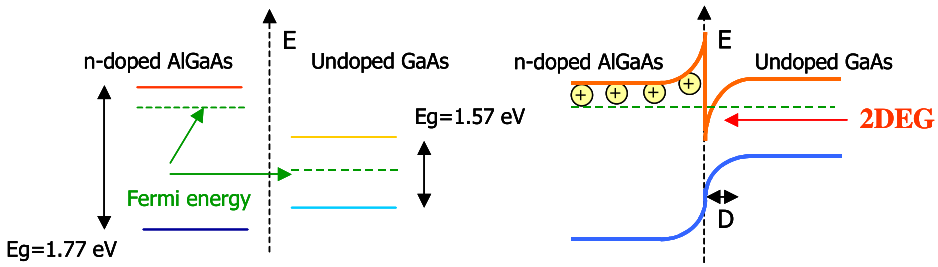

Fig. 9. Energy bands in a GaAs/AlGaAs heterostructure.

guidelines [29] that were deduced from a large number of metrological characterizations of QHE samples. These guidelines include recommendations about the geometry of the samples. A wide Hall bar channel increases the breakdown current of the QHE (Fig. 8a) and allows the sample to be biased with a large current while preserving the quantization of R_H and improving the signal to noise ratio of its measurement [30]. It is also recommended that samples have Hall voltage terminals with narrow arms perfectly aligned transversely to the current flow, as well as long conduction channels to favor the equilibration of the edge states occupancy. Low values of the contact resistances ($< 10\ \Omega$) and longitudinal resistances (typically less than 100 μΩ per square) are particularly crucial. Quantization is indeed related to the absence of backscattering, so in other words of dissipation. Fig. 8b displays a linear relationship between ΔR_H and R_{xx} over more than three decades [31]. An effective misalignment of voltage terminals resulting from the residual inhomogeneity [32] of the density of electrons or to the finite width of the probes combined with chirality of the edges states [33] explains this observation. In principle, R_H accurately reproduces R_K by extrapolation to the zero dissipation state.

3. Quantum resistance standards

3.1. Two-dimensional electron systems

The two-dimensional conductors required for the implementation of the QHE are usually two-dimensional electron gases (2DEG) obtained from different semiconductor technologies: Si-Mosfet, III–V or II–VI heterostructures. For now, samples based on GaAs/AlGaAs heterostructures are particularly appropriate to ohm metrology applications. These semiconductor systems also take benefit from a refined fabrication mastery acquired over more than forty years of development efforts. Fig. 9 explains the formation principle of a potential well. Two semiconductor layers with different energy gaps and doping levels are considered. The balance of their chemical potentials which occurs when the two layers come into contact requires that some electrons supplied by the Si-doped AlGaAs layer are transferred towards the GaAs layer. This transfer bends the valence and conduction bands and a potential deep with a triangular shape is formed at the layer interface on the GaAs side in which the electrons are caught. At the Fermi energy, the confining transverse width is approximately 10 nm, thus well below the Fermi wavelength (more than 50 nm).

The momentum quantization of the electrons in the well for a motion perpendicular to the interface leads to a sequence of 2D (surface) subbands. The energy level spacing between subbands, of the order of 0.1 eV, is much larger than the thermal energy corresponding to the cryogenic temperature at which QHE experiments are performed. Hence, only the lowest electronic subband is occupied. The dynamics of electrons is therefore two-dimensional. Fig. 10 shows an example of the vertical layer stacking which can be realized by molecular beam epitaxy (MBE) or metal organic chemical vapor

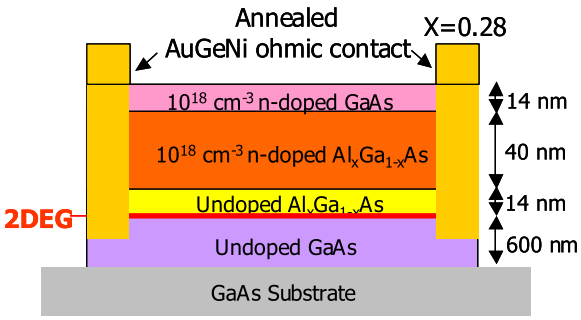

Fig. 10. Vertical stacking of layers in a GaAs/AlGaAs heterostructure.

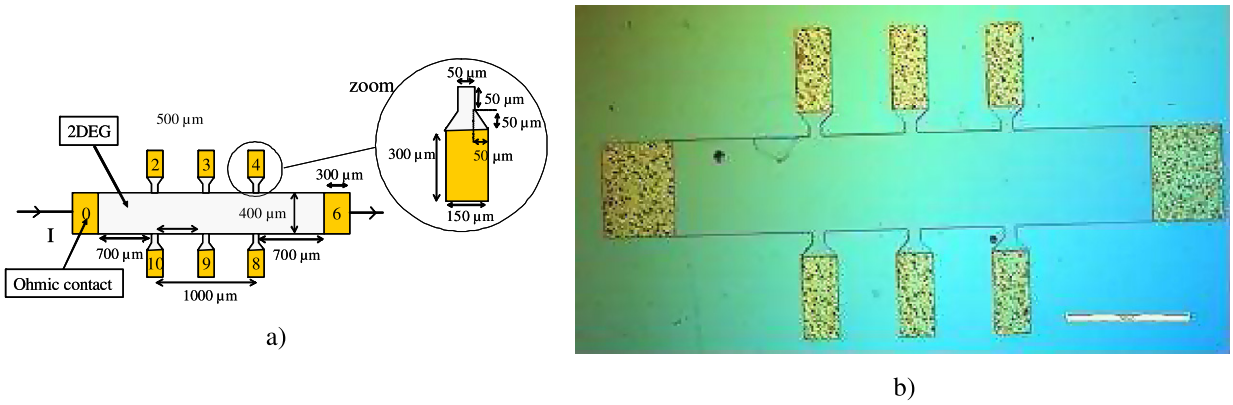

Fig. 11. a) Typical design of a Hall bar for the metrological application of quantum resistance standard. b) Photography of such a Hall bar fabricated in GaAs/AlGaAs 2DEG with Au/Ge/Ni ohmic contacts.

deposition (MOCVD). The spacer layer is used to increase the electronic mobility of the 2DEG by moving away the electrons from the ionized donor atoms. Electrical connection with the 2DEG is realized by annealing AuGeNi contacts. Obtaining ohmic contacts with very low resistances (about 10 Ω) as recommended by the technical guidelines is very challenging. For metrological applications, a density and a mobility of electrons in the range of 3 to 5×10^{15} m^{-2} and 10 to 50 T^{-1} are required respectively. These densities allow the $\nu = 2$ filling factor to be reached at large magnetic induction (about 10 T). This leads to a sufficiently higher cyclotron energy (energy spacing between Landau levels) than the thermal energy ($T = 1.5$ K) that ensures a quantization of R_H at the ppb level. The mobility range targeted gives an amount of disorder giving rise to large Hall plateaus (it has clearly been observed a shrinking of the Hall plateau when increasing the 2DEG mobility too much as shown in Fig. 2a). Finally, samples with Hall bar shapes can be fabricated by using optical lithography techniques [34]. The design is chosen to follow at best the metrological guidelines.

Even if GaAs/AlGaAs 2DEGs allow the fabrication of ppb-accurate quantum resistance standards, these devices require high magnetic field (10 T) and low temperature (1.5 K) for their operation, that is to say very costly experimental techniques. That is why the quest for a novel material enabling a more practical quantum resistance standard operating at higher temperature and lower magnetic field while keeping the accuracy is still continued. Graphene could lead to significant progress in this quest.

3.2. Single Hall bars

The simplest and historically the first system used for the metrological implementation of the QHE is the single Hall bar, which consists of a circuit with a rectangular aspect ratio and equipped with lateral contacts in addition to the contacts at the extremities. Such a sample is represented in Fig. 11. These elementary devices fabricated in GaAs/AlGaAs 2DEGs with properties as described above allow the practical realization of only two values of R_H sufficiently quantized to be used as references with an accuracy of the order of the ppb: the Hall resistance on the $\nu = 2$ plateau giving the reference $R_{K\text{-}90}/2 = 12\,906.4035$ Ω and on the $\nu = 4$ plateau giving the reference $R_{K\text{-}90}/4 = 6453.20175$ Ω.

3.3. Quantum Hall Array Resistance Standards (QHARS)

With the aim of having quantum resistance standards with more various values extending over a wide range (100 Ω to 1 MΩ), a particular engineering based on very fundamental properties of the QHE has been developed to design arrays

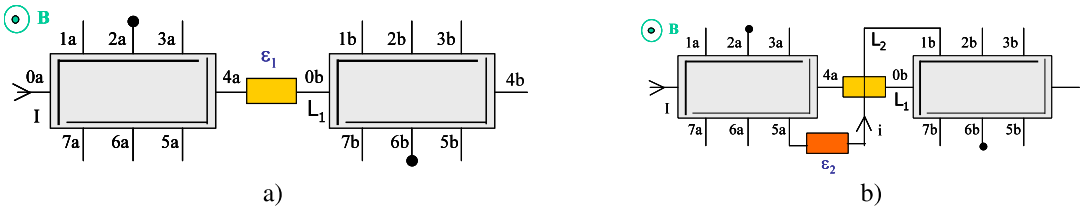

Fig. 12. a) Two simply series connected multiterminal Hall bars. b) Two doubly series connected multiterminal Hall bars.

combining a large number of Hall bars in series and/or parallel. This approach has been inspired by the same philosophy as that which led to the development of the Josephson Arrays Voltage Standards (JAVS). It has resulted in the development of Quantum Hall Arrays Resistance Standards (QHARS) which are acknowledged as being the core of the next generation of quantum resistance standards.

The basic principle of the realization of the QHARS is the multiple connection technique [26]. This technique consists in connecting multiterminal QHE devices with redundant links. It allows one to cancel the interconnection resistance effect and consequently to define the four-terminal resistance of any array made of several Hall bars while keeping the fundamental properties of the QHE. Let us consider two Hall bars connected by only one resistive link L_1 the resistance of which is expressed relatively to R_H by ε_1 ($\varepsilon_1 \ll 1$) (Fig. 12a). The voltage $V_{2a\text{-}6b}$ is given by:

$$V_{2a\text{-}6b} = V_{3a\text{-}7b} = V_{3a\text{-}5a} + V_{4a\text{-}0b} + V_{1b\text{-}7b} = R_H I + \varepsilon_1 R_H I + R_H I = 2R_H(1 + \varepsilon_1/2) \tag{10}$$

The discrepancy to $2R_H$ is thus proportional to ε_1. Due to the specific shape of equipotentials which results from chirality property, the voltage drop $V_{5a\text{-}1b}$ is equal to $V_{4a\text{-}0b}$. Short-circuiting $5a$ and $1b$ terminals by a second link L_2 (see Fig. 12b) makes circulate a small current i which is only a small fraction of the main current I because the resistance seen between $5a$ and $1b$ terminals is approximately $2R_H$ (the two-terminal resistance is R_H in QHE regime). Finally, the voltage $V_{2a\text{-}6b}$ is given by:

$$V_{2a\text{-}6b} = V_{3a\text{-}7b} = V_{3a\text{-}5a} + V_{5a\text{-}1b} + V_{1b\text{-}7b} = R_H I + \varepsilon_2 R_H i + R_H I = 2R_H I(1 + \varepsilon_1\varepsilon_2/4) \tag{11}$$

The discrepancy to $2R_H$ is thus proportional to $\varepsilon_1\varepsilon_2$ in case of double connection. Deviations to quantized value due to interconnection resistance effect are of order $O(\varepsilon^n)$, where n is the number of links. Considering interconnection resistance of 1 Ω, triple connection technique is enough to realize Quantum Hall Array Resistance Standards (QHARS) accurate [35,36] with an uncertainty of less than one part in 10^9.

The realization of QHARS mainly relies on the two-dimensional electron gas (2DEG) properties, notably its homogeneity, and on the quality of the electrical contact to it, like for the single Hall bars. In order to obtain operational QHARS, all the Hall bars must be in the same non-dissipative quantum state over a common magnetic field range. Unlike the Josephson Array Voltage Standards (JAVS), the design of the QHARS circuit based on the multiple connection technique is rather simple. However, the fabrication needs at least seven steps, all based on lithography: deposition of the contacts, realization of the vertically stacked redundant metallic links between the multiterminal Hall bars according to the multiple connection technique, etching of the 2DEG to define the Hall bars, etc. The quality of the layer which ensures the electrical insulation between two vertically stacked levels of metallic connections is particularly crucial: any short-circuit due to pinholes makes the device unusable. Its deposition has also to be without damage for the electronic properties of the 2DEG. A first generation of QHARS has been fabricated with values ranging, on the $\nu = 2$ Hall plateau, from about 100 Ω to about 1.29 MΩ, including 1.29 kΩ or 129 kΩ for example. Fig. 13a shows the picture of a QHARS129 sample [37]. It is composed of 100 Hall bars, 200 µm wide, placed in parallel by triple connections. Fig. 13b shows the magnetoresistance curves of two different arrays. The quality of the traces (both Shubnikov–de Haas oscillations for R_{xx} and Hall plateaus for R_H) is similar to that observed for a single metrological Hall bar. The accuracy of QHARS has been tested by several NMIs [38]. Following detailed investigations, it has been found that especially parallel low resistance QHARS could be perfectly quantized within 2 or 3 parts in 10^9. The accuracy of the Hall resistance of a series $50R_K$ (∼1.29 MΩ on the $\nu = 2$ plateau) QHARS has been verified with a measurement uncertainty of 20 parts in 10^9. Another way to realize a QHARS made of a large number of Hall bars connected in parallel consists in etching the array in a heterostructure with two stacked 2DEGs provided they have similar electronic densities (within a few %). A QHARS of $R_K/100$ nominal value fabricated in this way was accurate within 1 part in 10^8 [39]. The fabrication of such vertically stacked double 2DEG is still an issue and has been recently reproduced [40]. Thus, QHARS should open as many prospects to ohm metrology as JAVS brought to volt metrology. The wide range of the resistance values offered by these standards much better match the industrial needs. Low resistance value QHARS (for example $R_K/200$) stay quantized within an uncertainty of some parts in 10^9 with the bias currents of a few mA which make them compatible with commercial room temperature resistance bridges. Both features make QHARS very useful for the simplification and the shortening of the resistance calibration chain which are favorable to the reduction of the final measurement uncertainties. Arrays technology should also greatly improve the reproducibility of high-value resistance standards (for example $50R_K$). The QHARS have also been proved to be very useful for the test and calibration of all the resistance comparison bridges, including the commercial ones and the more specific CCC based bridges. High resistance value QHARS

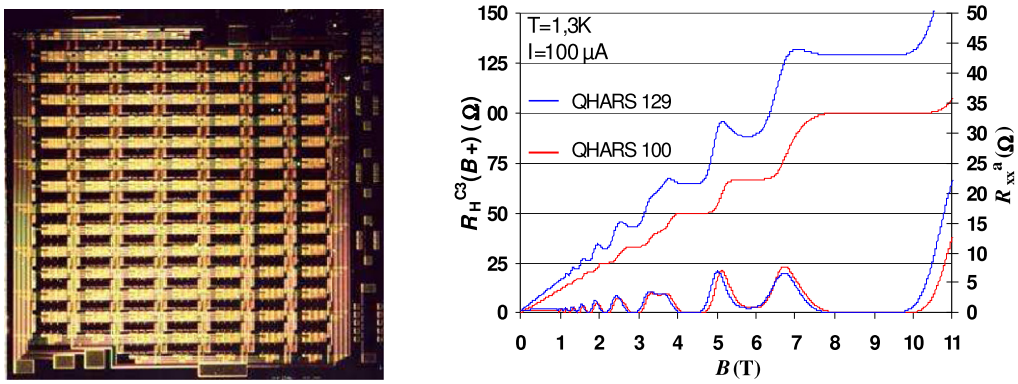

a) b)

Fig. 13. a) Picture of a QHARS129 (100 Hall bars set parallel to each others). b) Magnetoresistance curves for QHARS129 and QHARS100.

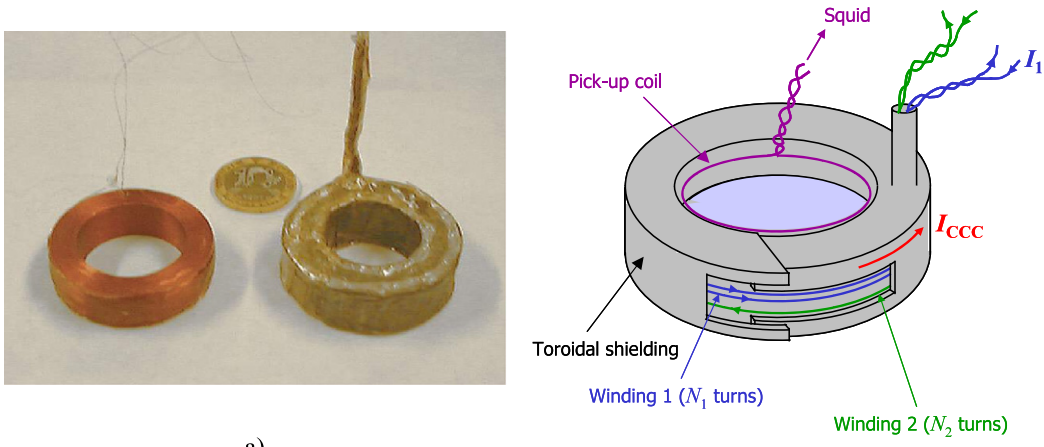

a) b)

Fig. 14. a) Pictures of CCCs. b) Drawing of a CCC.

are particularly useful for the measurement of the bridge leakages. Finally, with QHARS more accurate international resistance comparisons are expected: their universal and dematerialized nature, inherent to any quantum standard, reduces to zero the uncertainty component related to the instability of a traveling standard, which can be huge for a material resistor (>10 ppb). Thus, uncertainties of some parts in 10^9 as low as those obtained with direct comparisons can be targeted in such international comparisons, while avoiding the transportation of the QHE setup. More generally, the multiple connection technique allows the realization of many electrical circuits based on QHE like Wheatstone bridges and voltage dividers.

4. Calibration of resistance in direct current (DC) mode

Once the quantum standard is realized, wire resistors are calibrated by the use of resistance comparison bridges. Depending on the target uncertainty of the calibration, different bridges can be operated: commercial bridges based on direct current comparator, potentiometric bridges or specific bridges equipped with Cryogenic Current Comparator (CCC). The latter class of equipment gives the lowest measurement uncertainties. The cryogenic current comparator is a perfect transformer with a superconducting shield operating in DC [41] (Fig. 14). Its principle of operation is based on the Ampere theorem application and Meissner effect.

Fig. 14b shows a drawing of a CCC. Two windings of number of turns N_1 and N_2 fed by currents I_1 and I_2 respectively are placed in a superconducting torus which overlaps itself without electrical contact so that the screening current I_{CCC} is obliged to circulate from inside surface to outside surface along a close path. By this way, I_{CCC} can be detected by the pick-up coil connected to a Superconducting Quantum Interference Device (SQUID) throughout a flux transformer [42]. Applying Ampere theorem along a path within the superconducting material where $B = 0$ gives:

$$I_{CCC} = N_1 I_1 - N_2 I_2 \tag{12}$$

Table 2
CCC current resolution.

$S_{CCC}^{opt} = 4$ µA turn/ϕ_0	Current white noise ($N = 2000$ turns)	Current white noise ($N = 20\,000$ turns)
SQUID RF: $10^{-4}\phi_0/\mathrm{Hz}^{1/2}$	200 fA/Hz$^{1/2}$	20 fA/Hz$^{1/2}$
SQUID DC: $3\times10^{-6}\phi_0/\mathrm{Hz}^{1/2}$	6 fA/Hz$^{1/2}$	0.6 fA/Hz$^{1/2}$

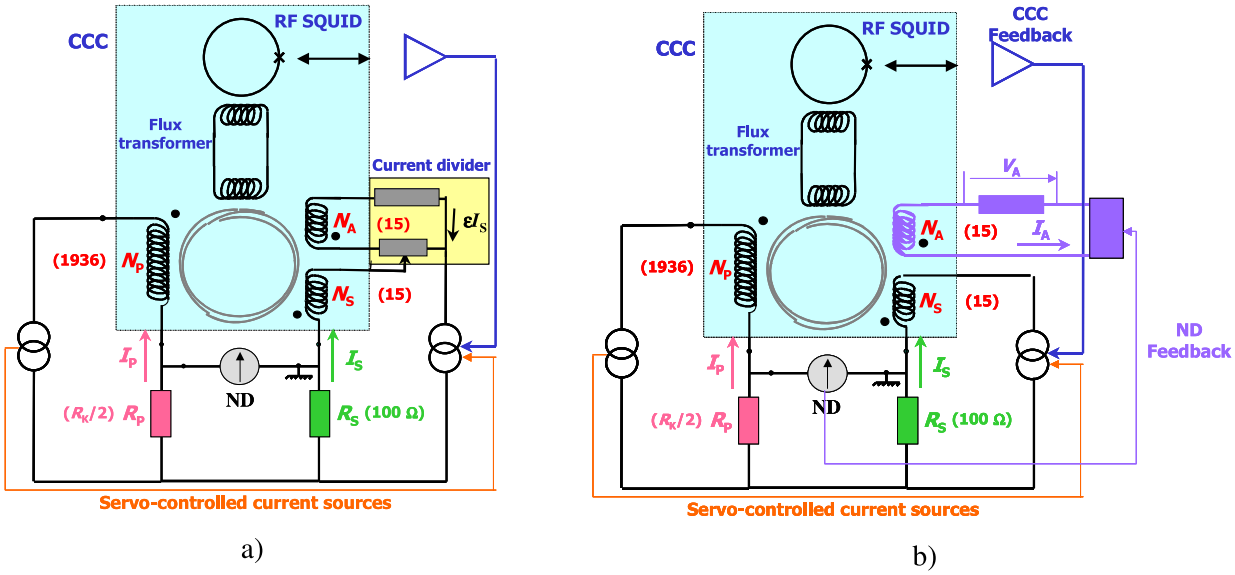

Fig. 15. a) Drawing of a resistance comparison bridge based on a CCC and a current divider. b) Drawing of a resistance comparison bridge based on a CCC, including an additional feed back between the auxiliary winding and the null detector.

A feedback technique which sets $I_{CCC} = 0$ by servo-controlling the current I_2 leads to $N_1 I_1 = N_2 I_2$. The ratio I_1/I_2 is therefore perfectly known in terms of the ratio N_1/N_2. In practice, the number of turns ratio can be accurate with a relative uncertainty lower than one part in 10^{10}. The sensitivity of the CCC is the supercurrent I_{CCC} circulating on the surface of the overlapping tube which creates, throughout a superconducting flux transformer, one flux quantum ϕ_0 across the SQUID ring. An optimal sensitivity as low as 4 µA turn/ϕ_0 can be experimentally achieved. Table 2 gives several current resolutions in fA/Hz$^{1/2}$ depending on the number of turns of the detecting winding and on the SQUID white noise level. With regards to these values, the CCC appears as a perfect amplifier in quasi DC regime with a current resolution which can be as low as 1 fA/Hz$^{1/2}$.

Fig. 15 shows drawings of two QHE resistance bridges based on a CCC [43]. For both bridges, two servo-controlled current sources supply the resistors R_P and R_S to be compared. The ratio of these currents I_P and I_S is roughly adjusted so that the difference between the voltages at the resistors terminals, measured by the null detector, is less than 10^{-5} of the voltage drop at the terminals of one resistor. I_P and I_S circulate across windings of number of turns N_P and N_S respectively. N_P and N_S are chosen so that the ratios N_P/N_S and R_P/R_S are close within some parts in 10^5. This choice ensures a low I_{CCC} current. In bridge of Fig. 15a, an auxiliary winding of number of turns N_A is supplied with a fraction ε of the current I_S by using a current divider. In external feedback mode I_S is regulated so that the supercurrent I_{CCC} is maintained to zero and ε is chosen so that the null detector measures zero voltage. This operation is described by two equations:

$$R_P I_P = R_S I_S \quad \text{and} \quad N_P I_P = N_S I_S (1 + \varepsilon N_A/N_S) \tag{13}$$

Thus:

$$\frac{R_S}{R_P} = \frac{N_S}{N_P}\left(1 + \varepsilon \frac{N_A}{N_S}\right) \tag{14}$$

The accuracy of this bridge technique is mainly based on the accuracy of the winding ratio and the current divider calibration. In bridge of Fig. 15b, the small current flowing in the auxiliary winding can also be provided by a feedback electronics controlled by the null detector signal instead of a current divider (Fig. 15b) [44]. By using such resistance comparison bridges, it is possible to calibrate a 100 Ω wire resistor in terms of $R_{K\text{-}90}$ with a relative uncertainty of 1 part in 10^9. To achieve such low uncertainties, it is essential to carry out measurements in a temperature regulated room which is also shielded against electromagnetic perturbations.

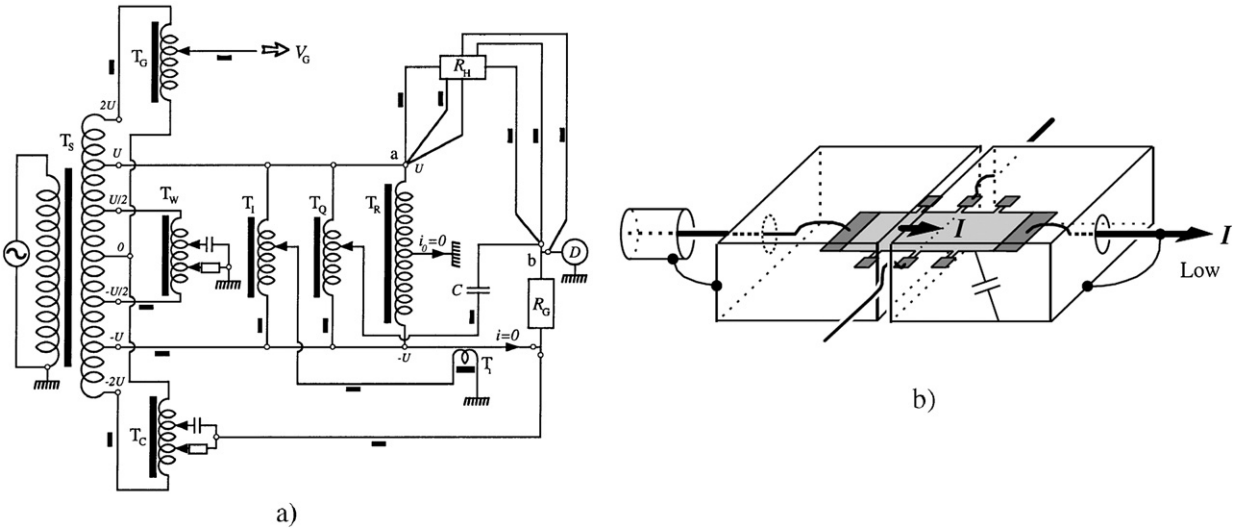

Fig. 16. a) Drawing of a resistance bridge used in AC regime from Ref. [48]. b) Shielding of a Hall for the application as quantum impedance standard in AC regime from Ref. [51].

5. Calibration of resistance in alternating current (AC) mode

Since no deviation of the Hall resistance from quantization is theoretically expected within one part in 10^9 [45,46] in the kilohertz range, metrologists work to operate the QHE in alternating current (AC) to realize an impedance standard. The implementation of the AC-QHE relies on the development of terminal-pair resistance bridges and quadrature bridges that are based on the coaxial measurement techniques [47]. However, it turns out that specific techniques have to be operated to preserve a perfect quantization of the Hall resistance. Firstly, the Hall bar is implemented using the multiple series connection technique. On one hand, this technique cancels large quadratic frequency dependencies due to series inductance, but also simplifies the bridge since zero current requirement in the voltage arm of the QHR is automatically ensured [48, 49] (Fig. 16a). Moreover, active equalizers are recommended to ensure a good coaxiality because of the high impedance of the shielding conductors connecting the QHR at low temperature. Despite of these precautions, several works show deviation ΔR_{H} of the Hall resistance from quantized value linearly increasing with frequency and measurement current [50]. A linear relationship between ΔR_{H} and R_{xx} is observed in AC as in DC regime except that the coupling factor is larger. This discrepancy is attributed to losses of AC charging current in internal capacitances of the Hall bar and in external capacitances of coupling with ground. Although some works propose that dielectric losses of samples layers are responsible for this phenomenon, the microscopic mechanism of dissipation remains not well understood. However, it is possible to cancel their impact on the Hall resistance to within about one part in 10^9 per kilohertz by using a double-shielding technique of the Hall bar (Fig. 16b) [51]. The operation of the QHE in AC regime at frequencies of some kilohertz therefore opens up the way towards a quantum standard of impedance [52,53]. It allows the calibration of the frequency correction of wire resistors or capacitances [54] without referring to calculable resistors [55,56]. Moreover, the measurement chains used for determining capacitance and R_{K}, which are based on quadrature bridge, should be shortened by starting from the AC-QHE instead of the DC-QHE (Fig. 21).

6. Direct determination of the von Klitzing constant, R_{K}, in the SI base units

6.1. Is R_{K} equal to h/e^2?

The present value of R_{K} in SI units as officialized by the CIPM is $R_{\mathrm{K\text{-}90}}$ within a relative uncertainty of 1 part in 10^7, thus three order of magnitudes larger than the reproducibility uncertainty of the QHE. This uncertainty was set in order to cover the discrepancies to $R_{\mathrm{K\text{-}90}}$ of the determinations of h/e^2 and of R_{K} directly calibrated with the Thompson–Lampard calculable capacitor [13]. An enlightening way to discuss the present agreement degree of the R_{K} and h/e^2 values consists in comparing all together the determinations of the fine structure constant α. Fig. 17 gathers the significant determinations of α as calculated by the CODATA group [57]. On one hand, h/m_{at} measurement [m_{at} is an atomic mass (Cs or Rb)] by atomic interferometry techniques [58] or measurement of the magnetic moment of the electron a_e introduced in quantum electrodynamics calculations [59] gives direct determinations with the lowest uncertainties of $\alpha = \mu_0 c/(2h/e^2)$. On the other hand, R_{K} determinations give an estimator $\alpha(R_{\mathrm{K}}) = \mu_0 c/2R_{\mathrm{K}}$ of α known with a relative uncertainty of 1.8×10^{-8}. Given their definitions, the agreement degree of the α and $\alpha(R_{\mathrm{K}})$ values determines the verification level of the relationship $R_{\mathrm{K}} = h/e^2$. As observed in Fig. 17, more accurate determinations of R_{K} are needed in order to check the equality within an uncertainty below 10^{-8}, which is the target uncertainty defined by an international consensus before proceeding to any

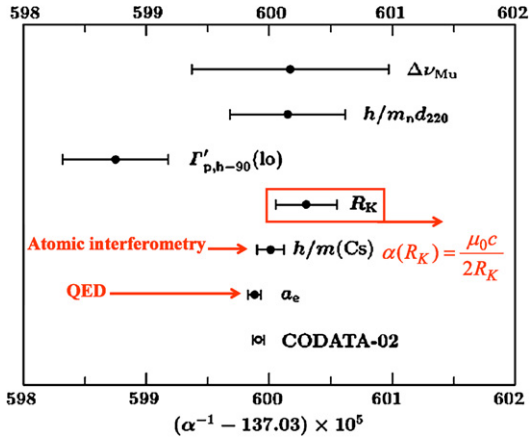

Fig. 17. CODATA 2006 determinations of α from Ref. [57].

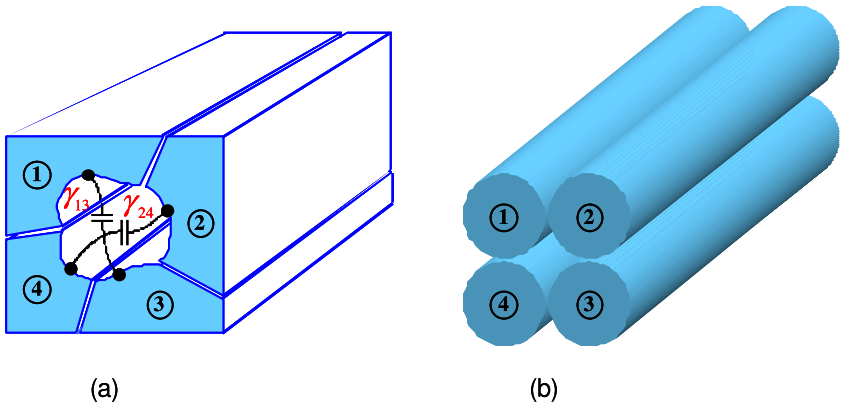

Fig. 18. a) and b) Four electrodes assemblies verifying the Thompson–Lampard theorem.

evolution towards an SI based on fundamental constants [60]. This requirement leads to the development of new Thompson–Lampard calculable capacitors by several national metrology institutes, and among them the LNE. Next subsections describe the LNE project of determination of R_K which is representative of those developed by others NMIs (NRC, CSIRO, BIPM, NIST) [61]. Although different, all experiments are built taking account of similar mechanical and electrical requirements.

6.2. The Thompson–Lampard theorem

A Thompson–Lampard calculable capacitor generates a calculable capacitance variation proportional to the displacement of a movable guard in its cross section, allowing one to link the farad to the meter. This result comes from the implementation of a theorem in electrostatics demonstrated by A. Thompson and D. Lampard in 1956 [13,62]. This theorem stipulates that for a cylindrical system composed of four isolated electrodes of infinite length and placed in vacuum (Fig. 18a), the direct cross capacitances per unit of length γ_{13} and γ_{24} between two opposite electrodes verify the relation:

$$\exp(-\pi\gamma_{13}/\varepsilon_0) + \exp(-\pi\gamma_{24}/\varepsilon_0) = 1 \tag{15}$$

where ε_0 is the permittivity of vacuum. This remains true whatever the shape of the inside cross section of the electrode assembly as the generating lines remain parallels. Moreover, in case of a perfect symmetry, the cross capacitances per unit of length are equal and it results that:

$$\gamma_{13} = \gamma_{24} = \gamma = (\varepsilon_0 \ln 2)/\pi \approx 1.953\,549\,043 \text{ pF/m} \tag{16}$$

and then a value of the electrical capacitance can be directly linked to a length measurement. On theoretical and practical point of views, electrodes of circular cross section is the best choice (Fig. 18b).

The Thompson–Lampard theorem has been extended to a system of five electrodes by N. Elnékavé in 1973 [63]. In such a configuration if one connects successively two adjacent electrodes, the five electrodes system is equivalent to five different four electrodes Thompson–Lampard capacitors by circular permutation (Fig. 19). In practice this leads to have an

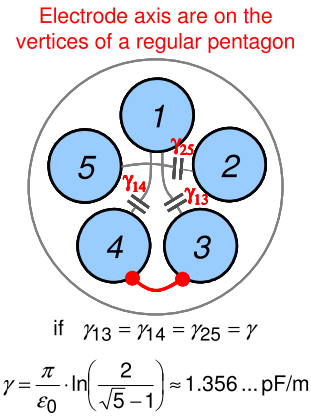

Fig. 19. Cross section of a five electrodes Thompson–Lampard capacitor with electrodes 3 and 4 connected.

over abundant number of equations to describe the system and the capacitance of the capacitor can be calculated with five different systems of equations.

The comparison of the five capacitance values obtained, which should be equal, gives information about the degree of perfection of the capacitor.

6.3. The new LNE Thompson–Lampard calculable capacitor

The last determination of R_K performed at LNE in 2000 has an uncertainty of 5.3 parts in 10^8. The uncertainty attributed to the calculable capacitor is about 4 parts in 10^8 and that of the measurement chain linking the calculable capacitor to dc resistance is about 2.5 parts in 10^8 [64]. In order to continue to actively take part in the necessary improvement of the SI, the LNE started in late 2005 a project aiming to build a new Thompson–Lampard calculable capacitor and to improve its comparison bridges in view of determining R_K with the target relative uncertainty of 10^{-8} [65].

The new LNE calculable capacitor has five cylindrical electrodes in vertical position arranged so that they stand at the vertices of a regular pentagon. They are made of non-magnetic stainless steel and their length and diameter are respectively 450 and 75.5 mm. These dimensions should allow capacitance variations up to 1 pF to be produced. The two prevailing uncertainty components among those due to the mechanical imperfections of the capacitor are: (1) the cylindricity defects of the cavity due to the departure of the electrodes shape from perfect cylinders and to their mispositioning with respect to each other; and (2) the coaxiality defect between the capacitor axis and the trajectory of the moving guard. It may be shown that, to reach the overall target uncertainty, the electrodes cylindricity and positioning defects must remain below 100 nm and that the movable guard trajectory may be controlled within 50 nm or less. These two points constitute obviously the main difficulties in designing and realizing such a capacitor. The mechanical structure of the new LNE calculable capacitor [66] is shown in Fig. 20. The electrodes (part (1)) are assembled vertically in a stiff frame (part (2)) equipped with positioning systems (part (3)) that allow the adjustment of their relative position with respect to the others so that they stand at the vertices of a regular pentagon within ±50 nm. Specific fabrication and measurement processes had to be implemented to realize electrodes with cylindricity defects less than 100 nm [67]. The electrodes are prolonged at both ends with cylindrical parts of same diameter (part (4)) but larger cylindricity defects. The usable length of the capacitor is then increased from 200 to 400 mm, thereby allowing capacitance variations between 0.3 pF and about 1 pF depending on the displacement length of the moving guard electrode (part (5)). An accurate measurement of this length is carried out with a Michelson interferometer not shown in Fig. 20. In order to make possible the alignment of the electrodes within 50 nm, a measuring machine (part (6)) is integrated in the capacitor structure. It allows to measure in situ the position of the electrodes during the alignment procedure with an accuracy better than 20 nm. The capacitor assembly is fitted on the main frame (part (7)) equipped with a lift system (part (8)) that enables to translate either the measuring machine along the electrodes or the moving guard electrode within the inter-electrode cavity. The whole parts of the mechanical structure are made of non-magnetic materials as well as the vacuum enclosure in which the whole assembly is located (10^{-3} Pa vacuum).

6.4. Direct measurement method of R_K

Several coaxial AC comparison bridges are used for the direct determination of R_K. The overall view of the successive measurements is shown in Fig. 21. The AC measurements are carried out at 3 angular frequencies $\omega = 2500$ rad/s, $\omega = 5000$ rad/s and $\omega = 10\,000$ rad/s [64]. Firstly, a 1 pF capacitor ($C_{1\,\mathrm{pF}}$) is compared to the Thompson–Lampard calculable capacitor with a two terminal-pair bridge [47] the ratio of which being adapted to the capacitance variation produced by the calculable capacitor. Then two 10:1 ratio bridges (two and four terminal-pair) are used successively to link two 10 000 pF

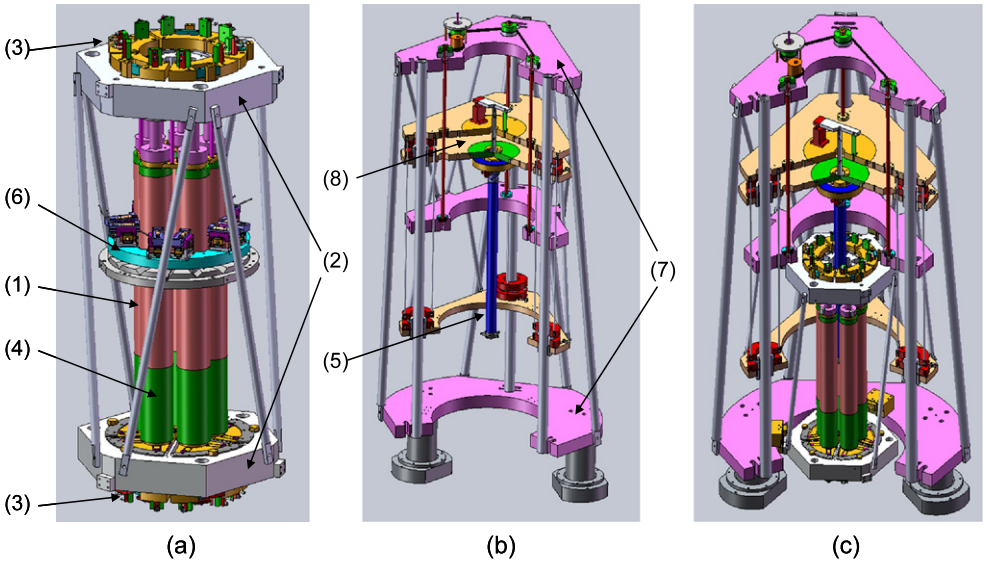

Fig. 20. a) Calculable capacitor structure. b) Main frame with the lift used to translate either the integrated measuring machine or the moving guard electrode. c) Complete mechanical assembly of the Thompson–Lampard capacitor. (1) Electrodes, (2) capacitor frame, (3) positioning systems of the electrodes, (4) electrode extensions, (5) moving guard electrode, (6) integrated measuring machine, (7) main frame, (8) lift system.

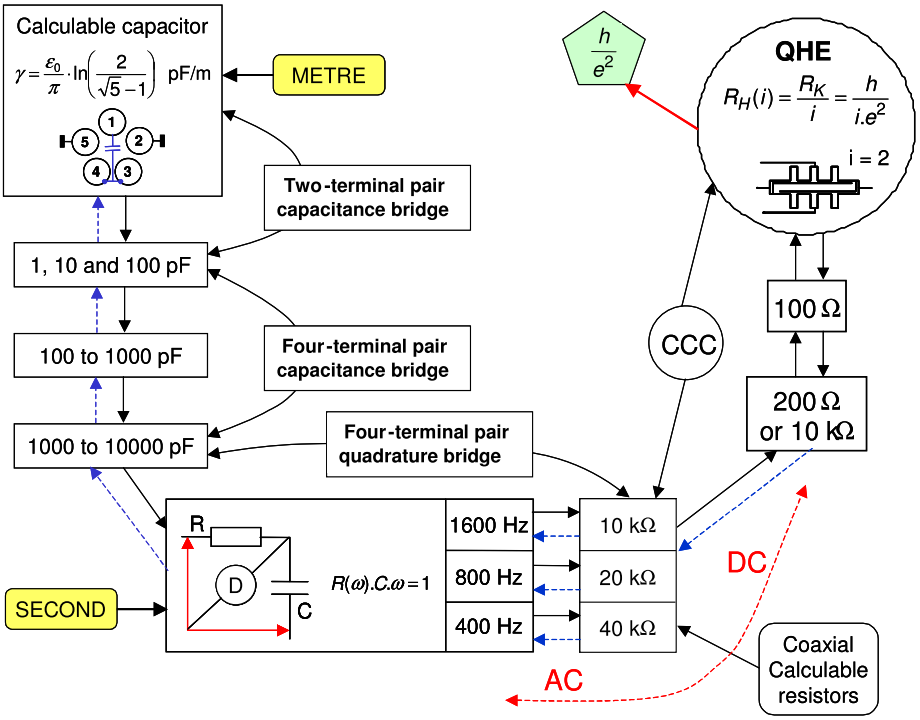

Fig. 21. Measurement method for the SI realization of the ohm and the determination of R_K.

capacitors (home made invar plates in vacuum capacitors) to the $C_{1\,\mathrm{pF}}$ capacitor. The 1000 pF transfer standard is nitrogen sealed capacitor placed in oil bath while the 100 and 10 pF transfer standards are thermoregulated fused silica capacitors (Andeen–Hagerling capacitors). Next, a quadrature bridge allows one to compare with a very high accuracy the impedances of the 10 000 pF capacitors (C_1 and C_2) to that of pair of resistors R_1 and R_2. Three couples of resistors are used with values of 40, 20 and 10 kΩ, the bridge being balanced ($R_1R_2C_1C_2\omega^2 = 1$) for the three angular frequencies mentioned above $\omega = 2500, 5000$ and $10\,000$ rad/s, respectively. After correction of their frequency variations, by means of AC/DC calculable resistance standards, the resistances are compared to the quantum Hall resistance standard in DC. This comparison is made using a CCC based resistance bridge (LNE). For the last determination of R_K, the more penalizing uncertainty components

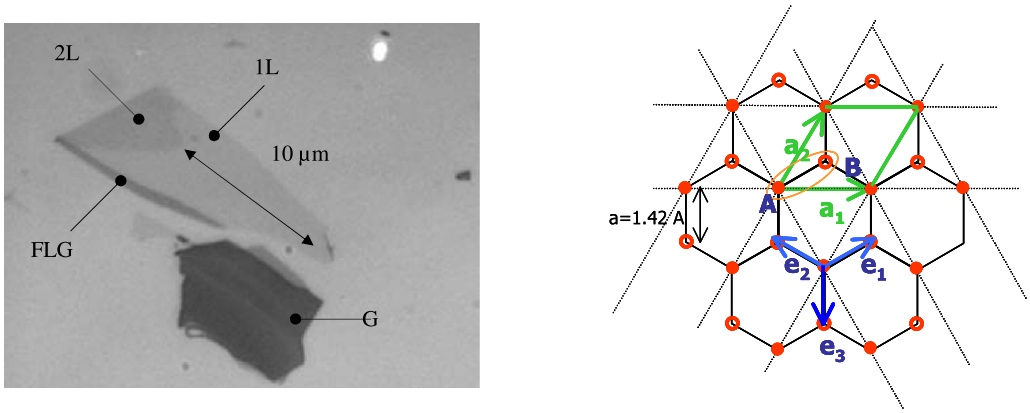

Fig. 22. a) Graphene layers on a Si/SiO_2 substrate: monolayer (1L), bilayer (2L), a few layers (FLG), graphite rock (G). b) Triangular Bravais lattice of graphene with a two-atom (A and B) basis: a is the atom spacing.

associated to the measuring chain are those related to the knowledge of the ratios of the AC bridges ($\approx 1.5 \times 10^{-8}$) and of the frequency dependence of the transfer resistors (≈ 1.1 to 1.7×10^{-8}). A big work has already been carried out to reduce the effect of the frequency dependence [68], and new two-stage voltage transformers with appropriate electrostatic and magnetic shields are being built. The uncertainty attributed to the measurement chain is expected to be decreased to a level close to 5×10^{-9} which should make possible a new determination of the von Klitzing constant with the targeted overall relative uncertainty of 10^{-8}.

7. Graphene and resistance metrology

7.1. Introduction

Graphene is a 2D crystallized carbon atoms monolayer with a honeycomb lattice [69]. This one atom thick material can be produced by mechanical exfoliation of natural graphite. Fig. 22a shows an optical picture of graphene monolayer, bilayer and a few layers obtained by this technique and then deposited on a Si/SiO_2 wafer. The number of layers can be determined by optical contrast or Raman spectroscopy analysis. The Si-doped layer can be used as a back gate to set the density of carriers in graphene layers by field effect. Graphene material can also be produced by chemical vapor deposition on metal [70] (like copper) or by annealing of silicon carbide [71].

The Bravais lattice of graphene is triangular with 2 carbon atoms per unit cell named A and B (Fig. 22b). Nearest to atoms A are three atoms B. The energy spectrum determined by tight-binding calculation gives two energy bands, the valence band (VB; $\alpha = -1$) and the conduction band (CB; $\alpha = +1$) which touch each other at zero energy at the corners of the hexagonal First Brillouin Zone (FBZ) [69,72,73] (Fig. 23a). There are only two inequivalent points K^- and K^+ named Dirac points. For undoped graphene, the valence band (lower energy) is full, the conduction band is empty, so the Fermi energy is at zero energy. Thus, undoped graphene is a semiconductor with a zero energy gap and two valleys. Around the K points, the band structure is conical. A low energy expansion valid for energies much lower than the nearest neighbor hoping energy t ($\varepsilon \ll t = 2.7$ eV) gives a linear energy dispersion

$$\varepsilon_{p,\alpha} = \alpha \frac{3ta}{2} |p| = \alpha v_F |p| \quad \text{with } p \text{ impulsion and} \quad v_F = \frac{3ta}{2\hbar} \quad \left(v_F \approx 10^6 \text{ m/s}\right) \tag{17}$$

Because of the two different sites A and B, the low energy effective Hamiltonian expanded around K^+ (valley index $\xi = +1$) and K^- (valley index $\xi = -1$) Dirac points has a 2×2 structure:

$$i\hbar\partial_t |\psi\rangle = H^\xi |\psi\rangle, \quad |\psi\rangle = \begin{pmatrix} \psi_A \\ \psi_B \end{pmatrix}, \qquad H^\xi(p) = \xi v_F \begin{pmatrix} 0 & p_x - ip_y \\ p_x + ip_y & 0 \end{pmatrix} = \xi v_F p.\sigma \tag{18}$$

where $\sigma = (\sigma_x, \sigma_y)$ are Pauli matrices.

This particular low energy physics is responsible for the relativistic character of quasi-particles involved in the transport properties [74–76]. The Fermi velocity v_F plays the role of the "speed of light". The effective mass of electrons is zero at Dirac points. Carriers behave like massless Dirac fermions with chirality property characterized by a Berry's phase π. Physics around these points can be explored moving the Fermi energy by biasing the backgate. At the charge neutrality point a peak of resistivity occurs and simultaneously the charge sign of carriers reverses as displayed by Hall resistance measurement (see Fig. 23b). Carrier mobilities up to 20 000 $cm^2\,V^{-1}\,s^{-1}$ were measured in exfoliated graphene deposited on Si/SiO_2 substrate. The record mobilities have been measured in freely suspended graphene layers where they approach 200 000 $cm^2\,V^{-1}\,s^{-1}$

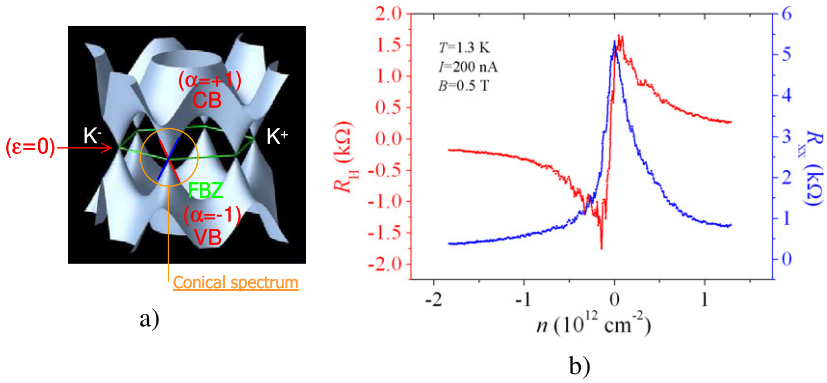

Fig. 23. a) Electronic band structure of monolayer graphene. b) Typical variations of the Hall and longitudinal resistances in a graphene sample as a function the charge carriers density (varied by electrical field effect).

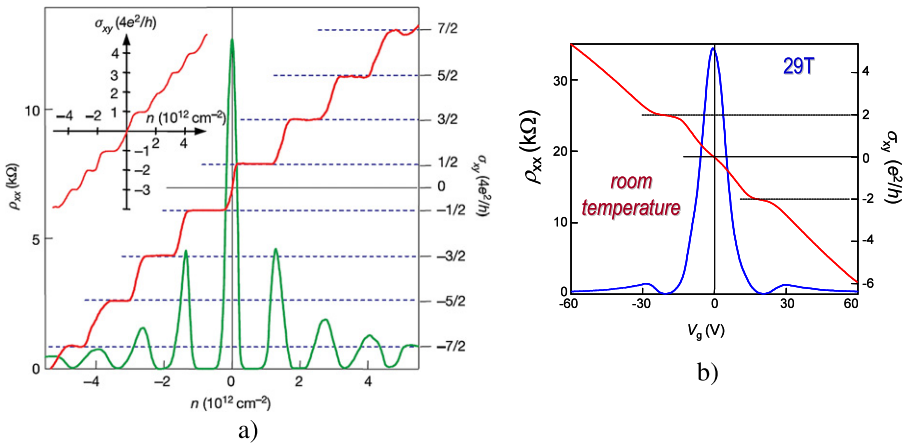

Fig. 24. a) QHE in monolayer graphene and bilayer graphene (insert) from Ref. [80]. b) Observation of the QHE at room temperature from Ref. [82].

at room temperature, thus overcome those measured in any semiconductor. The fractional quantum Hall effect was recently observed in such suspended graphene layers [77,78]. In graphene bilayer which consists of two graphitic monolayer arranged according to Bernal stacking, the low energy dispersion relation becomes parabolic and carriers behaves like massive chiral Dirac fermions (effective mass $m^* = 0.033m_e$) with Berry's phase 2π. This 2DEG system offers a unique physics which is the object of intensive fundamental research in itself. More generally, graphene systems are of great interest for high speed electronics applications due to high Fermi velocities. The opportunity to have an energy gap in nanoribbons (also in bilayer graphene by applying an electrical field) could be even exploited for digital transistors [79].

7.2. Quantum Hall effect in graphene

The QHE in monolayer and bilayer graphene produced by exfoliation was observed in 2005 by two different groups [80,81]. Fig. 24a shows the transverse conductivity σ_{xy} and longitudinal resistivity ρ_{xx} *versus* carrier density at $T = 4$ K and $B = 14$ T. The QHE is half-integer for monolayer graphene and the resistivity curve exhibits a peak of finite height at zero density which indicates a zero energy Landau level. Although the integer quantum Hall effect is recovered in bilayer graphene, a zero energy Landau level also manifests itself (see insert Fig. 24a). The QHE in graphene layers is so robust that under magnetic field density higher than 29 T the first plateau is still observable at 300 K [82] as shown in Fig. 24b. These specific features of the QHE reflect the chirality property of Dirac carriers in graphene systems. They can be explained by considering the Landau level energies. They are given by calculating the eigenvalues of the graphene (monolayer or bilayer) Hamiltonian in presence of a magnetic field [69,83,84] which is obtained by introducing a vector potential A in the Hamiltonian without magnetic field (Eq. (18)) through the substitution $p \to \prod = p + eA$.

Table 3 sums up the main features of the physics of graphene systems and GaAs in presence of magnetic field in case of spin and valley (for graphene) degeneracy. In monolayer graphene, the energy of Landau levels varies as the root square of Bn instead of B in semiconductors. Thus, the energy gap between Landau levels reduces with the index number n. The degeneracy of each Landau level is $4eB/h$ (two spin directions and two valley values). The anomalous half integer sequence of Hall plateau is related to the fact that the zero energy Landau level is half filled for zero carrier density $n_s = 0$. In bilayer graphene, the energy of Landau levels scales linearly with B as in semiconductors and energy gaps quickly

Table 3
Comparison of the QHE in monolayer, bilayer graphene and GaAs 2DEG.

System	Monolayer Graphene	Bilayer Graphene	GaAs/AlGaAs
Band structure at low E (B=0)	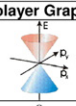	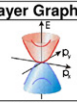	
Quasiparticle mass	0	$0.033\ m_e$	$0.067\ m_e$
Berry's phase	π	2π	0 (non chiral)
Hamiltonian	$H_{\pm} = \pm v_F(\vec{p} + e\vec{A})\vec{\sigma}$	$H_{\pm} = \pm\vec{\sigma}.\frac{1}{2m^*}(\vec{p} + e\vec{A})^2$	$H = \frac{1}{2m^*}(\vec{p} + e\vec{A})^2$
Landau level energy	$\varepsilon_n = \pm\sqrt{2\hbar v_F^2 e.\sqrt{nB}}$	$\varepsilon_n = \pm\hbar\omega_c.\sqrt{n(n-1)}$	$\varepsilon_n = \hbar\omega_c.(n + \frac{1}{2})$
Density of states	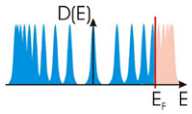	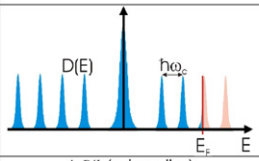	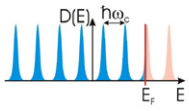
Degeneracy	$4eB/h$ (spin+valley)	$4eB/h$ (spin+valley) and twice higher at E=0	$2eB/h$ (spin)
Hall resistance plateaus	$R_H = \pm\frac{1}{4(\nu+1/2)}\cdot\frac{h}{e^2},\ \nu \geq 0$	$R_H = \pm\frac{1}{4\nu}\cdot\frac{h}{e^2},\ \nu > 0$	$R_H = \frac{1}{2\nu}\cdot\frac{h}{e^2},\ \nu > 0$
First LL energy spacing (meV) and equiv. temp. (K)	$\sqrt{2\hbar v_F^2 eB} = 39.8\sqrt{B[\mathrm{T}]}$ (meV) $\equiv 462\sqrt{B[\mathrm{T}]}$ (K)	$\hbar\omega_c.\sqrt{2} = 4.94\times B[\mathrm{T}]$ (meV) $\equiv 57.3\times B[\mathrm{T}]$ (K)	$\hbar\omega_c = 1.72\times B[\mathrm{T}]$ (meV) $\equiv 20\times B[\mathrm{T}]$ (K)
First LL energy spacing at 1T	39.8 meV / 462 K	4.94 meV / 57.3 K	1.72 meV / 20 K
First LL energy spacing at 20T	178.2 meV / 2066 K	98.9 meV / 1147 K	34.4 meV / 399.3 K

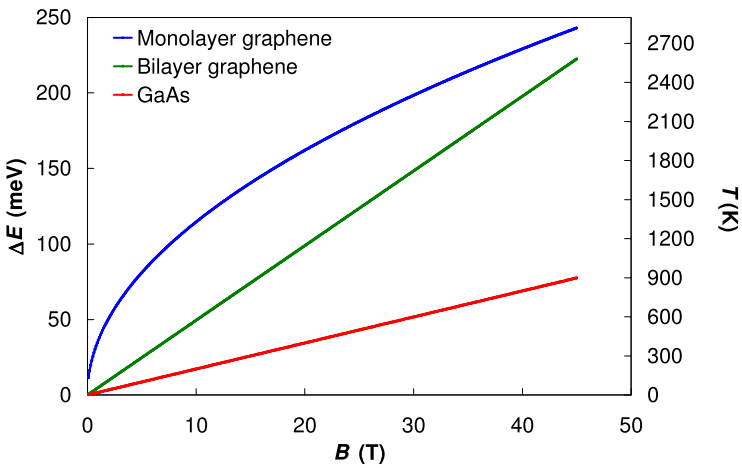

Fig. 25. Energy gap (in meV and in equivalent temperature) between the two first Landau levels in monolayer graphene, bilayer graphene and in GaAs based 2DEG.

tend to $\hbar\omega_C$ for increasing n index. Moreover, $n = 0$ and $n = 1$ Landau levels are degenerated which results in a $8eB/h$ degeneracy at zero energy. Numerical values indicated in Table 3 show that the energy spacing between first Landau levels in monolayer graphene is much larger than in GaAs, particularly at low magnetic induction. This explains the observation of the QHE quantization at 300 K, and generally speaking suggests that the Hall quantization in graphene should be very robust. Graphene material appears particularly suitable for developing a quantum resistance standard working at higher temperature, under lower magnetic induction, and with higher measurement current (compared to GaAs). Bilayer graphene also seems to be very promising for resistance metrology since the energy gap between first Landau levels is larger than in GaAs although it is lower than in monolayer (see Fig. 25). Therefore, it appears crucial to test the merit of both graphene materials as candidate for the QHE metrology. Moreover, the underlying physics in both 2DEG systems being very different from that of semiconductors, a comparison of quantum resistance standards fabricated with these different materials would give a stringent test of the QHE universality. Furthermore the verification of the universal character of the von Klitzing constant R_K (theoretically equal to h/e^2) would considerably support the setting up of a *Système International* (SI) of units based on fundamental constants of physics [14].

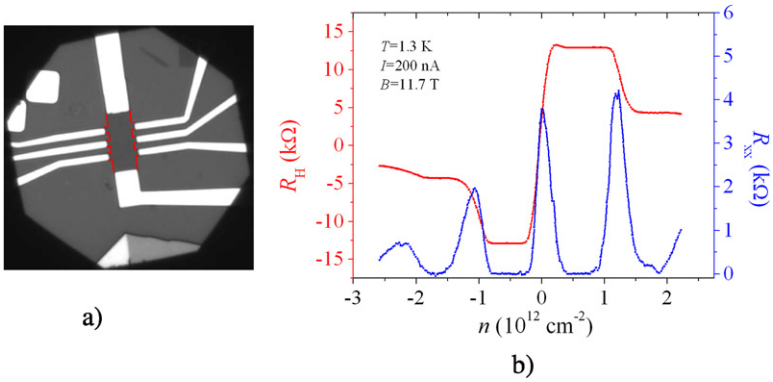

Fig. 26. a) Photography of a graphene Hall bar connected with metallic contacts. The width of the channel is 3 µm. The contour is emphasized by red lines. b) Typical variations of the Hall and longitudinal resistances in a graphene sample as a function the charge carriers density (varied by electrical field effect) at high magnetic field. The Hall plateaus $\nu = \pm 2$ and ± 6 are clearly visible. (For interpretation of the references to color in this figure legend, the reader is referred to the web version of this article.)

7.3. First metrological works

Metrological studies of the QHE in graphene has started in samples fabricated by mechanical exfoliation of graphite [84] since this quantum phenomena was unobservable in epitaxial graphene until recently [85–88]. It turns out to be a challenge to develop a graphene based quantum resistance standard that fulfills metrological requirements. As discussed in Section 2.3, a perfect quantization at the 10^{-9} level, which is the target, relies on several properties of the Hall bar sample: good contacts (typically below 100 Ω), largest channel width to benefit from a large breakdown current, a geometry of voltage and current terminals that ensures a weak coupling between the Hall resistance and the longitudinal resistance. Fulfilling these requirements using the exfoliation technique, notably implies to select only biggest graphene layers and to develop an adequate sample design for each selected layer. Fig. 26a shows a typical design of Hall bar dedicated to metrological characterization. After exfoliation and optical location, the sample is realized using *e*-beam lithography techniques combined to Cr/Au, Ti/Au or Pd contacts deposition and oxygen plasma etching of graphene. Fig. 26b shows measurements of the Hall resistance R_H and longitudinal resistance R_{xx} *versus* carrier density performed in a graphene Hall bar under high magnetic induction. It displays $\nu = \pm 2$ and $\nu = \pm 6$ Hall resistance plateaus which are typical of monolayer graphene.

The first accurate measurements of the QHE which was performed with a Hall bar device made of exfoliated monolayer graphene found an agreement of the Hall resistance with $R_K/2$ ($\nu = 2$ plateau) within an uncertainty of 15 parts in 10^5 [89]. This uncertainty is large with regards to the use of a CCC based resistance bridge for the measurement. It was mostly caused by the high contact resistance (some kΩ) of the metal electrodes attached to the graphene and to the low breakdown current (< 2 µA). The small size of the sample (about 10 µm^2) which is typical of exfoliated graphene devices, contributes to both the high contact resistance and the low breakdown current. This is a major disadvantage of the exfoliation technique for resistance metrology application.

Besides, all NMIs carrying out studies of the QHE in exfoliated graphene have been faced with bad and fragile contacts, but also strong inhomogeneity of the carrier density, both altering the quantization. Nevertheless, quantization tests of the QHE with a measurement accuracy of some parts in 10^7 were achieved in Hall bars samples made of either monolayer graphene ($B = 11.7$ T, $T = 1.5$ K) or bilayer graphene ($B = 18.5$ T, $T = 0.35$ K) obtained by exfoliation [90]. This performance which shows that an accurate quantization can be observed in graphene, notably results from the realization of better contacts (some tens of ohms). But it is limited by the small size of the samples and the strong inhomogeneity of the carrier density. In these experiments the sample were covered by PMMA polymer in order to protect graphene layer from contamination by ad-atoms. Before measurement, an annealing to about 110 °C under vacuum was performed to further decrease the residual density of carriers and increase the carrier mobility. Despite previous unsuccessful attempts to observe the QHE in epitaxial samples, a large improvement of the measurement accuracy of the QHE quantization was reported in a large area sample of graphene grown by epitaxy on silicon carbide. In a large Hall bar (160×35 µm^2) with low resistance connecting pads (about 1 Ω), the Hall resistance measured with a 12 µA current at 300 mK and 14 T magnetic induction was found to agree with $R_K/2$ within 3 parts in 10^9 (see Fig. 27) [88]. This result relies on a breakthrough in fabrication: annealing the silicon carbide under 1 atm of argon rather than in vacuum leads to the growth of large-area single monolayer graphene of better structural quality on the Si-terminated face of the substrate. Moreover, carrier densities of less than 10^{12} cm^{-2} and mobilities of about 5000 cm^2 V^{-1} s^{-1} are obtained. The observation of the QHE in single layer epitaxial graphene was demonstrated by others works [91,92]. Carrier mobilities up to 20 000 cm^2 V^{-1} s^{-1} were reached in graphene growth on C-face of 4H silicon carbide [91]. All these results give hope that graphene could challenge the role of GaAs in future quantum standards. Moreover, the epitaxial growth of graphene on silicon carbide [71] or by chemical vapor deposition on metals [70] seems to be compatible with existing manufacturing processes. This is an asset for the metrology application. Although further basic technological work is needed to realize a more practical resistance standard, graphene

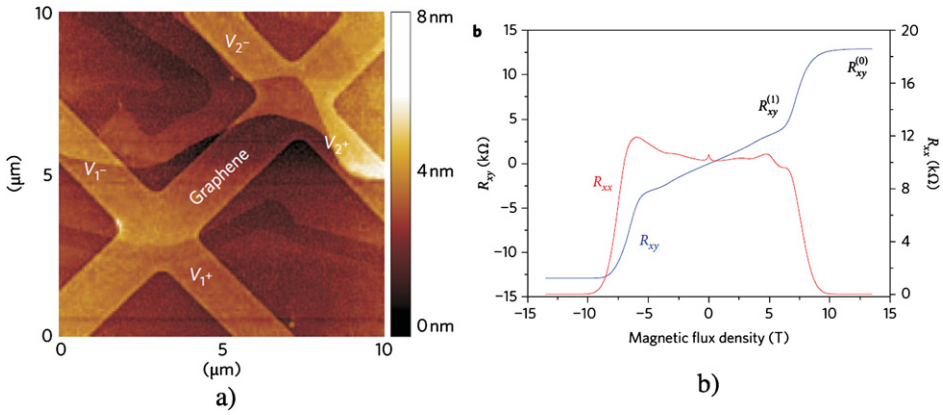

Fig. 27. a) Hall bar sample fabricated in monolayer graphene obtained by epitaxy on the Si-terminated face of SiC. b) QHE magnetoresistance curves obtained in a large epitaxial graphene sample. Figures from Ref. [88].

material keeps one's promises until now. An increase of the carrier mobility, a better control of the carrier density and of its homogeneity will be crucial to operate graphene based quantum resistance standard cooled down at 4 K with a helium free cryocooler under a magnetic induction of only some teslas.

8. Conclusion

The representation of the unit of resistance based on the QHE is universal: the ohm can be maintained in each NMI with a relative uncertainty of one part in 10^9. Owing to the multiple connection technique, quantization properties of the QHE can be preserved in various electrical circuits: accurate Quantum Hall Array Resistance Standards (QHARS), voltage dividers, Wheatstone bridge. The latter is particularly suitable for realizing new universality tests of the QHE with a target uncertainty less than 10^{-11}. The application of this technique also allows the operation of the QHE with an alternating current in the kilohertz range with an accuracy of some parts in 10^{-9}. This opens the way towards a quantum standard of impedance. In the context of the future revising of the *Système International* of units, the QHE is the cornerstone of three main experiments: the R_K determination, the watt balance experiment and the metrological triangle experiment. Their results should lead to the determination of the constants involved in quantum metrology with a relative uncertainty as low as one part in 10^8. Finally, the QHE metrology is renewed by the emerging graphene topic. First quantization tests of the QHE show that graphene keeps one's promises and could challenge GaAs material in the development of a more practical quantum resistance standard.

References

[1] K.V. Klitzing, G. Dorda, M. Pepper, Phys. Rev. Lett. 45 (1980) 494.
[2] Comité International des Poids et Mesures, Recommandation 2 (CI-1988), in: 77th Session, 1988.
[3] KCDB database, Key comparison BIPM.EM-K12, BIPM, Sèvres, 2000.
[4] W. Poirier, F. Schopfer, in: F. Piquemal, B. Jeckelmann (Eds.), Quantum Metrology and Fundamental Constants, Eur. Phys. J. Spec. Top. 172 (2009) 207.
[5] W. Poirier, F. Schopfer, Internat. J. Modern Phys. B 23 (12–13) (2009) 2779.
[6] B. Jeanneret, S.P. Benz, in: F. Piquemal, B. Jeckelmann (Eds.), Quantum Metrology and Fundamental Constants, Eur. Phys. J. Spec. Top. 172 (2009) 181.
[7] N. Feltin, F. Piquemal, in: F. Piquemal, B. Jeckelmann (Eds.), Quantum Metrology and Fundamental Constants, Eur. Phys. J. Spec. Top. 172 (2009) 267.
[8] M.W. Keller, in: F. Piquemal, B. Jeckelmann (Eds.), Quantum Metrology and Fundamental Constants, Eur. Phys. J. Spec. Top. 172 (2009) 297.
[9] F. Piquemal, B. Jeckelmann (Eds.), Quantum Metrology and Fundamental Constants, Eur. Phys. J. Spec. Top. 172 (2009).
[10] B.P. Kibble, in: J.H. Sanders, A.H. Wapstra (Eds.), Atomic Masses and Fundamental Constants, vol. 5, Plenum Press, New York, 1976, p. 545.
[11] R.L. Steiner, E.R. Williams, D.B. Newell, R. Liu, Metrologia 42 (2005) 431.
[12] A. Eichenberger, G. Genevès, P. Gournay, in: F. Piquemal, B. Jeckelmann (Eds.), Quantum Metrology and Fundamental Constants, Eur. Phys. J. Spec. Top. 172 (2009) 363.
[13] A.M. Thompson, D.G. Lampard, A new theorem in electrostatics and its application to calculable standards capacitance, Nature 177 (1956) 888.
[14] W. Poirier, F. Schopfer, Nature Nanotechnol. 5 (2010) 171.
[15] M. Büttiker, Phys. Rev. B 38 (1988) 9375.
[16] D. Yoshioka, The Quantum Hall Effect, Springer-Verlag, Berlin, 2002.
[17] R.B. Laughlin, Phys. Rev. B 23 (1981) 5632.
[18] Q. Niu, D.J. Thouless, Y. Wu, Phys. Rev. B 31 (1985) 3372.
[19] F.W. Hehl, et al., Phys. Rev. Lett. 93 (2004) 096804-1.
[20] A.A. Penin, Phys. Rev. B 79 (2009) 113303.
[21] A.A. Penin, Phys. Rev. Lett. 104 (2010) 097003.
[22] A. Hartland, et al., Phys. Rev. Lett. 66 (1991) 969.
[23] B. Jeckelmann, A.D. Inglis, B. Jeanneret, IEEE Trans. Instrum. Meas. 44 (1995) 269.
[24] F. Delahaye, et al., Metrologia 22 (1986) 103.
[25] B. Jeckelmann, B. Jeanneret, Rep. Progr. Phys. 64 (2001) 1603.
[26] F. Delahaye, J. Appl. Phys. 73 (1993) 7914.

[27] F. Schopfer, W. Poirier, J. Appl. Phys. 102 (2007) 054903.
[28] F. Schopfer, W. Poirier, in: A.H. Cookson, T. Winter (Eds.), Proceeding of the Conference on Precision Electromagnetic Measurements, Boulder, 2008, p. 22.
[29] F. Delahaye, B. Jeckelmann, Metrologia 40 (2003) 217.
[30] B. Jeckelmann, et al., IEEE Trans. Instrum. Meas. 50 (2001) 219.
[31] M.E. Cage, et al., Phys. Rev. B 40 (1984) 2286.
[32] D. Domingez, PhD thesis, CNAM, Paris, 1987.
[33] W. van der Wel, C.J.P.M. Harmans, J.E. Mooij, J. Phys. C 21 (1988) L171.
[34] D. Mailly, in: F. Piquemal, B. Jeckelmann (Eds.), Quantum Metrology and Fundamental Constants, Eur. Phys. J. Spec. Top. 172 (2009) 333.
[35] F. Piquemal, et al., IEEE Trans. Instrum. Meas. 48 (1999) 296.
[36] W. Poirier, et al., J. Appl. Phys. 92 (2002) 2844.
[37] W. Poirier, A. Bounouh, F. Piquemal, J.P. André, Metrologia 41 (2004) 285.
[38] R. Goebel, et al., in: F. Levi, et al. (Eds.), Proceedings of the Conference on Precision Electromagnetic Measurements, Torino, 2006, p. 514.
[39] A. Bounouh, W. Poirier, F. Piquemal, G. Genevès, J.P. André, IEEE Trans. Instrum. Meas. 52 (2003) 555.
[40] K. Pierz, et al., Appl. Phys. Lett. 92 (2008) 133509.
[41] I.K. Harvey, Rev. Sci. Instrum. 43 (1972) 1626.
[42] J.C. Gallop, F. Piquemal, in: J. Clarke, et al. (Eds.), The SQUID Handbook, vol. II. Applications of SQUIDS and SQUID Systems, Wiley–VCH, Weinheim, 2006, p. 95.
[43] F. Delahaye, D. Reymann, IEEE Trans. Instrum. Meas. 34 (1985) 316.
[44] A. Hartland, Metrologia 29 (1992) 175.
[45] F. Kuchar, R. Meisels, G. Weimann, W. Schlapp, Phys. Rev. B 33 (1986) 2965.
[46] O. Viehweger, K.B. Efetov, J. Phys.: Condens. Matter 3 (1991) 1675.
[47] B.P. Kibble, G.H. Rayner, Coaxial AC Bridges, Adam Hilger Ltd, Bristol, 1984.
[48] F. Delahaye, Metrologia 31 (1995) 367.
[49] F. Overney, B. Jeanneret, B. Jeckelmann, IEEE Trans. Instrum. Meas. 52 (2003) 574.
[50] F.J. Ahlers, B. Jeanneret, F. Overney, J. Schurr, B.M. Wood, Metrologia 46 (2009) 1.
[51] B.P. Kibble, J. Schurr, Metrologia 45 (2008) 25.
[52] F. Overney, B. Jeanneret, B. Jeckelmann, B.M. Wood, J. Schurr, Metrologia 43 (2006) 409.
[53] J. Schurr, F.J. Ahlers, G. Hein, K. Pierz, Metrologia 44 (2007) 15.
[54] J. Schurr, V. Bürkel, B.P. Kibble, Metrologia 46 (2009) 619.
[55] R.J. Haddad, PhD thesis, George Washington University, 1969.
[56] D.L.H. Gibbings, Proc. IEEE 110 (1963) 335.
[57] P.J. Mohr, B.N. Taylor, D.B. Newell, Rev. Mod. Phys. 80 (2008) 633.
[58] P. Cladé, et al., Phys. Rev. A 102 (2006) 052109.
[59] D. Hanneke, S. Fogwell, G. Gabrielse, Phys. Rev. Lett. 100 (2008) 120801.
[60] BIPM (Eds.), Proc. Verb. Com. Int. Poids et Mesures, 93, 2004, p. 219, http://www.bipm.org.
[61] H. Bachmaier, in: F. Piquemal, B. Jeckelmann (Eds.), Quantum Metrology and Fundamental Constants, Eur. Phys. J. Spec. Top. 172 (2009) 257.
[62] D.G. Lampard, J. Inst. Electr. Eng. 104C (1957) 271.
[63] N. Elnékavé, Bull. BNM 13 (1973) 3.
[64] G. Trapon, et al., Metrologia 40 (2003) 159.
[65] P. Gournay, O. Thevenot, L. Dupont, J.M. David, F. Piquemal, Can. J. Phys. 89 (1) (January 2011) 169–176.
[66] P. Gournay, et al., in: Yang Sup Song (Ed.), Proceedings of the Conference on Precision Electromagnetic Measurements, Daejeon, 2010, p. 545.
[67] O. Thévenot, et al., in: Yang Sup Song (Ed.), Proceedings of the Conference on Precision Electromagnetic Measurements, Daejeon, 2010, p. 418.
[68] C. Conséjo, et al., IEEE Trans. Instrum. Meas. 58 (2009) 902.
[69] A.H. Castro Neto, F. Guinea, N.M.R. Peres, K.S. Novoselov, A.K. Geim, Rev. Mod. Phys. 81 (2009) 109.
[70] X. Li, et al., Science 324 (2009) 1312.
[71] C. Berger, et al., J. Phys. Chem. B 108 (2004) 19912.
[72] P.R. Wallace, Phys. Rev. 71 (1947) 622.
[73] K.S. Novoselov, A.K. Geim, S.V. Morozov, D. Jiang, Y. Zhang, S.V. Dubonos, I.V. Grigorieva, A.A. Firsov, Science 306 (2004) 666.
[74] A.K. Geim, K.S. Novoselov, Nature Mater. 6 (2007) 183.
[75] M.I. Katsnelson, K.S. Novoselov, A.K. Geim, Nature Phys. 2 (2006) 620.
[76] M.I. Katsnelson, K.S. Novoselov, Solid State Commun. 143 (2007) 3.
[77] X. Du, et al., Nature 462 (2009) 192.
[78] K.I. Bolotin, et al., Nature 462 (2009) 196.
[79] J. Nilsson, A.H. Castro Neto, F. Guinea, N.M.R. Peres, Phys. Rev. B 78 (2008) 045405.
[80] K.S. Novoselov, A.K. Geim, S.V. Morozov, D. Jiang, M.I. Katsnelson, I.V. Grigorieva, S.V. Dubonis, A.A. Firsov, Nature 438 (2005) 197.
[81] Y.B. Zhang, Y.W. Tan, H. Stormer, P. Kim, Nature 438 (2005) 201.
[82] K.S. Novoselov, Z. Jiang, Y. Zhang, S.V. Morozov, H.L. Stormer, U. Zeitler, J.C. Maan, G.S. Boebinger, P. Kim, A.K. Geim, Science 315 (2007) 1379.
[83] M.O. Goerbig, P. Lederer, Lecture Notes in French, University of Paris 11, 2006.
[84] V.P. Gusynin, V.P. Sharapov, Phys. Rev. Lett. 95 (2005) 146801.
[85] T. Shen, J.J. Gu, M. Xu, Y.Q. Wu, M.L. Bolen, M.A. Capano, L.W. Engel, P.D. Ye, Appl. Phys. Lett. 95 (2009) 172105.
[86] X. Wu, Y. Hu, M. Ruan, N.K. Madiomanana, J. Hankinson, M. Sprinkle, C. Berger, W.A. De Heer, Appl. Phys. Lett. 95 (2009) 223108.
[87] J. Jobst, D. Waldmann, F. Speck, R. Hirner, D.K. Maude, T. Seyller, H.B. Weber, Phys. Rev. B 81 (2010) 195434.
[88] A. Tzalenchuk, et al., Nature Nanotechnol. 5 (2010) 186.
[89] A.J.M. Giesberg, et al., Appl. Phys. Lett. 93 (2009) 222109.
[90] J. Guignard, et al., in: Yang Sup Song (Ed.), Proceedings of the Conference on Precision Electromagnetic Measurements, Daejeon, 2010, p. 577.
[91] X. Wu, et al., Appl. Phys. Lett. 95 (2009) 223108.
[92] T. Shen, et al., Appl. Phys. Lett. 95 (2009) 172105.